Time-reversal Imaging in Inhomogeneous Media

Part 3 Essay

Set by: Dr Orsola Rath-Spivack

Contents

Chapter 1

Introduction

In time reversal experiments, a signal emitted from a localised source is recorded, time-reversed, and retransmitted into the medium. The re-transmitted signal than refocuses onto the original source.

Time reversal imaging is a highly flexible and applicable principle which can provide information about a region while assuming no knowledge of the propagating medium. This makes it particularly useful in natural mediums and it has exciting and wide ranging applications to healthcare, communications, engineering, seismology and of course imaging.

This essay takes a very broad approach to the subject, focusing on applications and experiments while providing mathematical explanations to explain the phenomena observed. It is not an essay that looks at lemmas and proofs purely for their beauty or simplicity, although that is not to say the results aren't sometimes satisfying, but rather for their many and wide ranging applications.

We start, in the next section, Section 2, by broadly describing the principles of time reversal and some quantitative theories that underpin it. We consider possible experimental configurations and look at some of the benefits and limitations of time reversal methods.

In Section 3, we move on to look at potential extensions of the method. In most applications the original "source", that we wish to investigate, is not a source of waves, but rather a scatterer which will reflect an initial probing wave. We look at cases where there are multiple scatterers in the medium and I will describe an iterative method for focusing on an individual scatterer and methods for the imaging of point scatterers and measurements of their reflectivity.

In Section 4 we then look at the phenomenon of 'Super Resolution', where the focusing of the time reversed wave is actually improved in a random medium which is contrary to the intuitive idea of a loss of information because of an averaging effect of multiple scattering. We discuss qualitative and quantitative explanations for the phenomena before finally considering the difficulties of imaging in a random medium.

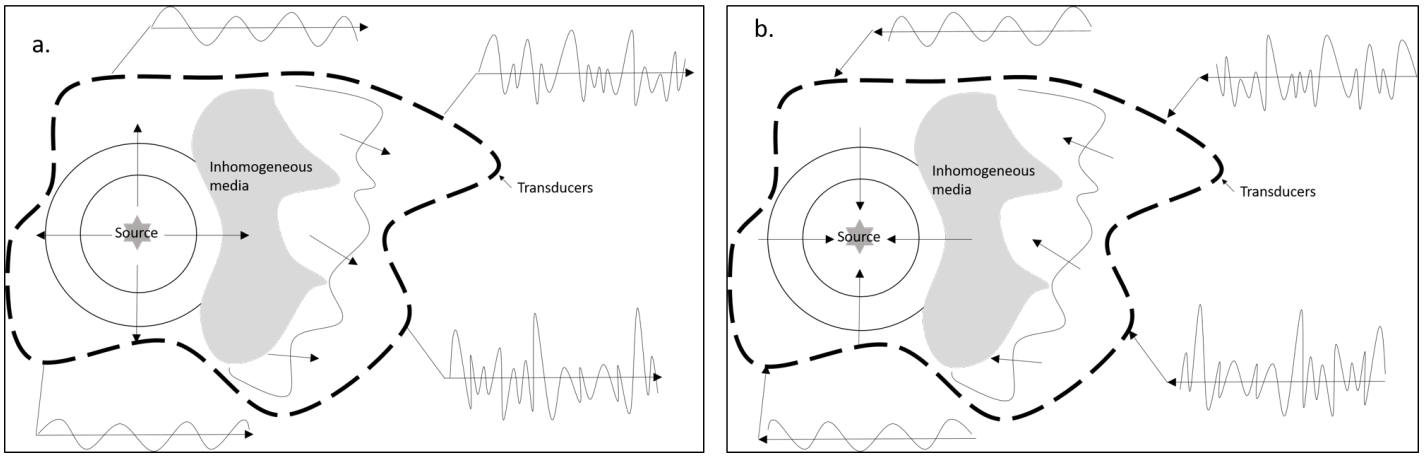

Figure 1.1: The two steps of time-reversal in a time reversal cavity. Diagrams inspired by Figure 4 in Paper [11]

Chapter 2

Introduction to Time-reversal

In this Section we will introduce the idea of time-reversal and show from first principles how it works. We will look at some of the benefits and limitations of time reversal before considering some applications.

2.1 Time Reversal Focusing

Time reversal focusing consists of two steps. In the first step, a source, inside a medium, emits sound waves that propagate out, perhaps being distorted by inhomogeneities in the medium. The resulting field is recorded over a period of time. In the second step, the recording is time reversed and re-emitted by an array of transducers, re-creating the original wave but travelling backwards. It retraces its passage back through the medium, untangling its distortions and refocuses on the original source point.

From a mathematical perspective, time reversal is possible because, in a lossless medium the wave linearised Equation has only second order time-derivatives:

$$\nabla^2 p - \frac{1}{c^2}\frac{\partial^2 p}{\partial t^2} = 0 \tag{2.1}$$

where c is the sound speed. Hence if $p(\mathbf{x}, t)$ is a solution then $p(\mathbf{x}, -t)$ is also a solution.

We will be considering the case of scalar waves, usually acoustic, and from an practical, engineers perspective, time reversal is possible because the record and transmit functions can be combined into a single device, most commonly a piezoelectric transducer. It converts sound into a voltage, which can be recorded, when the wave passes, and vibrates to produce pressure wave when a voltage signal is applied across it .

2.1.1 Time-Reversal Cavity

Time reversal focusing sounds brilliant! But with further thought, we realise it is not possible to sample a whole 3-D volume at every possible point point. We instead consider a closed surface surrounding the volume and measuring the field and its normal derivative on this surface will give us knowledge of the field in the whole volume. We call the volume enclosed by the surface the time reversal cavity.

The two steps of time reversal focusing, are now shown in Figure 1.1. First recording the pressure field at all points on the closed surface[1] and then the second step, creating secondary sources on the surface which corresponds to the time-reversal of the signals measured during the first step.

Lemma 2.1.1. *Consider an arbitrary (not necessarily spherical) 2-D closed surface, S, which is a time reversal mirror and the boundary of a volume, V. If, the volume V contains a point like source located at point $\boldsymbol{r}_0$, which emits a pulse at $t = t_0 \geq 0$, then the time reversed wave is of the form:*

$$\phi^{TR}(\boldsymbol{r}, t) = G(\boldsymbol{r}, T - t|\boldsymbol{r}_0, t_0) - G(\boldsymbol{r}, t|\boldsymbol{r}_0, T - t_0) \tag{2.2}$$

[1] As described in Paper [13] we don't actually need to measure the normal derivative: each transducer is set up so it records the incoming field in the forward direction and then retransmits it in the backward direction. The change between the forward and backward direction deals with the normal derivative of the field

where $G(\boldsymbol{r}, t|\boldsymbol{r}_0, t_0)$ is the background Green's function.

Proof. We follow Section 1.1 in Paper [13]. A point like source emits a pulse at $t = t_0 \geq 0$ and the resulting scalar wave is denoted by $\phi(\mathbf{r}, t)$ and satisfies the Equation:

$$\nabla \cdot \left(\frac{1}{\rho(\mathbf{r})}\nabla\right)\phi(\mathbf{r}, t) - \kappa(\mathbf{r})\frac{\partial^2\phi(\mathbf{r}, t)}{\partial t^2} = -A\delta(\mathbf{r} - \mathbf{r}_0)\delta(t - t_0) \tag{2.3}$$

where: A is a dimensionality constant that we can omit for now, $\rho(\mathbf{r})$ is the density of the medium and $\kappa(\mathbf{r})$ is the compressibility of the medium. It is a variation on Equation 2.1. The solution is the Green's function $G(\mathbf{r}, t|\mathbf{r}_0, t_0)$. If we are in free-space with a homogeneous background media the Green's function would be a diverging spherical impulse wave given by

$$G(\mathbf{r}, t|\mathbf{r}_0, t_0) = \frac{1}{4\pi|\mathbf{r} - \mathbf{r}_0|}\delta\left(t - t_0 - \frac{|\mathbf{r} - \mathbf{r}_0|}{c}\right). \tag{2.4}$$

We don't wish to make assumptions abut the background media, however, so we assume the Green's function is unknown. We do note that by causality $G(\mathbf{r}, t|\mathbf{r}_0, t_0) = 0$ for $t < t_0$ and that it is singular for $t = t_0$ and $\mathbf{r} = \mathbf{r}_0$ but that it is finite at all other points. We also note the reciprocity theorem which will be used repeatedly in this essay:

Reciprocity Theorem The position of a point source and an observer can be reversed without altering the observed acoustic pressure. Equivalently:

$$G(\mathbf{r}, t|\mathbf{r}_0, t_0) = G(\mathbf{r}_0, t|\mathbf{r}, t_0). \tag{2.5}$$

The pressure field and its normal derivative is measured at all points on the surface S for a sufficiently long time period $[0, T]$ such that the information loss can be considered negligible [2].

We now move onto the second step of the process, the time reversal process $t \to T - t$. We assume that we have removed the source from the domain and thus can use the Green's function of the background media at all points in the volume. We consider the sources to now be all points, **r'**, on the surface S:

$$\phi_S(\mathbf{r'}, t) = G(\mathbf{r'}, T - t|\mathbf{r}_0, t_0) \tag{2.6}$$

$$\partial_n\phi_S(\mathbf{r'}, t) = \partial_n G(\mathbf{r'}, T - t|\mathbf{r}_0, t_0) \tag{2.7}$$

A time reversed pressure field propagates in the cavity and can be given by the Helmholtz-Kirchhoff integral[3]:

$$\phi^{TR}(\mathbf{r}, t) = \int_{-\infty}^{+\infty} dt' \int\int_S G(\mathbf{r}, t|\mathbf{r'}, t')\partial_n\phi_S(\mathbf{r'}, t') - \phi_S(\mathbf{r'}, t')\partial_n G(\mathbf{r}, t|\mathbf{r'}, t')\frac{d^2\mathbf{r'}}{\rho(\mathbf{r'})} \tag{2.8}$$

We can then use Green's Second Identity

$$\int_V \left[\psi\,\nabla\cdot(\varepsilon\,\nabla\varphi) - \varphi\,\nabla\cdot(\varepsilon\,\nabla\psi)\right]\,dV = \oint_{\partial V}\varepsilon\left(\psi\frac{\partial\varphi}{\partial\mathbf{n}} - \varphi\frac{\partial\psi}{\partial\mathbf{n}}\right)\,dS\,. \tag{2.9}$$

Where we set:

- $\psi = G(\mathbf{r}, t|\mathbf{r'}, t')$
- $\varphi = \phi_S(\mathbf{r'}, t')$
- $\varepsilon = 1/\rho(\mathbf{r'})$

[2] In fact this assumption isn't necessary if the sound speed is constant and the spatial dimension is odd because Huygens' principle holds, which states that for any initial source with a bounded support, the wave leaves any bounded domain in a finite time i.e. there is a time, T, such that the solution vanishes inside inside the domain for any $t > T$ (if interested see Paper [15]).

[3] For reference consider any standard course or text book on wave scattering, including the lecture course [19]

and hence

$$\phi^{TR}(\mathbf{r},t)=\int_{-\infty}^{+\infty}dt'\int_V\left[G(\mathbf{r},t|\mathbf{r'},t')\nabla\cdot\left(\frac{1}{\rho(\mathbf{r'})}\nabla\phi_S(\mathbf{r'},t')\right)-\phi_S(\mathbf{r'},t')\nabla\cdot\left(\frac{1}{\rho(\mathbf{r'})}\nabla G(\mathbf{r},t|\mathbf{r'},t')\right)\right]d^3\mathbf{r'} \tag{2.10}$$

where ∇ is acting on the $\mathbf{r'}$.

The appearance of the term $\nabla\cdot\left(\frac{1}{\rho(\mathbf{r'})}\nabla\cdot\right)$ suggests that we return to Equation 2.3 for which $G(\mathbf{r'},t|\mathbf{r},t')$ and $\phi_S(\mathbf{r'},t')$ are both solutions (considering $\mathbf{r}$ and t constant and $\mathbf{r'}$ and t' varying):

$$\nabla\cdot(\frac{1}{\rho(\mathbf{r'})}\nabla G(\mathbf{r'}),t'|\mathbf{r},t)=\kappa(\mathbf{r'})\frac{\partial^2G(\mathbf{r'},t'|\mathbf{r},t)}{\partial t'^2}-\delta(\mathbf{r'}-\mathbf{r})\delta(t-t') \tag{2.11}$$

$$\nabla\cdot(\frac{1}{\rho(\mathbf{r'})}\nabla\phi_S(\mathbf{r'},t'))=\kappa(\mathbf{r'})\frac{\partial^2\phi_S(\mathbf{r'},t')}{\partial t'^2}-\delta(\mathbf{r'}-\mathbf{r}_0)\delta(T-t'-t_0) \tag{2.12}$$

We can almost plug both of these back in to Equation 2.10 but the Green's function in 2.10 Equation is of the form $G(\mathbf{r},t|\mathbf{r'},t')$ not of the form $G(\mathbf{r'},t'|\mathbf{r},t)$ in Equation 2.11. But we recall reciprocity and time reversal realise that they are in fact equal. Subbing these equations in to get:

$$\begin{aligned}\phi^{TR}(\mathbf{r},t)=\int_{-\infty}^{+\infty}dt'\int_V G(\mathbf{r},t|\mathbf{r'},t')[\kappa(\mathbf{r'})\frac{\partial^2\phi_S(\mathbf{r'},t')}{\partial t'^2}-\delta(\mathbf{r'}-\mathbf{r}_0)\delta(T-t'-t_0)]\\ -\phi_S(\mathbf{r'},t')[\kappa(\mathbf{r'})\frac{\partial^2G(\mathbf{r'},t|\mathbf{r},t')}{\partial t'^2}-\delta(\mathbf{r'}-\mathbf{r})\delta(t-t')]d^3\mathbf{r'}\end{aligned} \tag{2.13}$$

We assume that the pressure fields are negligible as $t\to\pm\infty$, hence when integrating by parts the boundary terms can be ignored and we find that the second order time derivatives cancel:

$$\begin{aligned}\phi^{TR}(\mathbf{r},t)=-\int_{-\infty}^{+\infty}dt'\int_V G(\mathbf{r},t|\mathbf{r'},t')[\delta(\mathbf{r'}-\mathbf{r}_0)\delta(T-t'-t_0)]d^3\mathbf{r'}\\ +\int_{-\infty}^{+\infty}dt'\int_V\phi_S(\mathbf{r'},t')[\delta(\mathbf{r'}-\mathbf{r})\delta(t-t')]d^3\mathbf{r'}.\end{aligned} \tag{2.14}$$

Which can be evaluated as:

$$\phi^{TR}(\mathbf{r},t)=\phi_S(\mathbf{r},t)-G(\mathbf{r},t|\mathbf{r}_0,T-t_0) \tag{2.15}$$

$$=G(\mathbf{r},T-t|\mathbf{r}_0,t_0)-G(\mathbf{r},t|\mathbf{r}_0,T-t_0) \tag{2.16}$$

□

Remark 1. This can be interpreted, as in Paper [13], as the superposition of incoming and outgoing spherical waves centred no the initial source position. The singularities of both waves occur at $t=T-t_0$.

The Green's function on the left hand side is an exact time reversal of the initial wave produced at $\mathbf{r}_0$. It traces the same route as the forward wave only backwards, focusing on the location of the original source.

The second term is a divergent wave with no contribution until after $t=T-t_0$, where it is an exact replica of the initial wave propagated from the source. It seems therefore that we haven't got an exact time reversal. Indeed if we imagined watching a film of the experiment in rewind the wave would converge and become singular at the point and then appear to be absorbed by the source where in our case the equations seem to suggest bouncing off the source. This has a logical explanation: an exact time reversal would include replacing the source by a sink whereas in our calculations we simply removed the source. This is why this term appears and why we are safe to ignore it.

We therefore conclude we get an exact refocusing in a time reversal cavity.

2.1.2 Practicalities of the Time Reversal Cavity and Other Configurations

The last Section sounds too good to be true and indeed a closed time reversal cavity cannot be realised experimentally or practically. There are two main reasons for this, given in Paper [7]:

- The transducers have a finite aperture so it is not possible to measure the pressure field at all points on the surface leading to an information loss. As mentioned in multiple papers, including Paper [13], information loss can be minimised by placing transducers a distance of $\lambda/2$ apart, where λ is the smallest wavelength of the pressure field.
- It is normally impossible to completely surround the region of interest: e.g.if you are attempting (non-destructively) test for cracks or inhomogeneities in a concrete wall it is only possible to to place transceivers on one side of the region of interest.

A more realistic set up would be an array of transducers located on one side of the region of interest, only a small part of the field is captured and time reversed, limiting reversal and focusing quality. This will be the main focus of Chapter 4.

Another interesting set-up is described in Paper [13], where waves propagate in a closed irregularly shaped reflecting cavity. If the cavity has negligible absorption then, given sufficient time, the random nature of reflections off the boundary of the cavity means that a single transducer may be able to collect the same amount of information as had we had a closed time reversal cavity. A potential medium would be silicon wafers because of the weak absorption of silicon. Mathias Fink, in an article in Scientific American [12], suggested that a message could be encrypted by sending out a wave, encrypting the message, from a source A, at a point in a irregular cavity and recording over a period of time with a transducer at B. The recording, which would be incoherent noise could then be made public. Someone who then knew the exact positions of A and B could then time reverse the signal, emit it from B and the original wave would be recreated at A. Someone who attempted to decode the signal without knowing A and B would only get a noisy mess.

Thus far we have only considered, static arrays. Paper [4] suggests the idea of a dynamic time reversal mirror (TRM), where it is possible to move the TRM laterally to capture as much energy, and thus information as possible. Numerically, this has been shown to increase resolution in some cases although there are cases where the energy is so spread out that it has little effect.

Ergodic cavities and dynamic TRMs are both interesting ideas, although maybe not the most practical, but unfortunately I don't have the time to return to them in this essay.

2.2 Benefits and limitations

2.2.1 Advantages

We start by considering two alternatives for focusing so that the advantages and limitation of the time-reversal technique have some context.

Paper [11] describes **adaptive time delay focusing techniques**. Transducers in an array measure the pressure waves coming from a point source. Points in the array are naturally at different distances from the source. Neighbouring transducers receive the signals with a small time difference and this can be analysed to determine the optimum time-delay characteristic required to focus on the source. Absurdly simplified: if it takes longer for a signal to move from a source to transducer A than from the source to transducer B then, to focus on the source, transducer A should emit a signal before transducer B to ensure the waves meet at the same time.

A simple technique to describe but it has two main issues[4]:

- Targets may not be point size and indeed in most applications they are not even regular, e.g. a kidney stone. This means that signals received by neighbouring transducers vary not only

[4]It is not to be completely dismissed, however; Paper [5] describes the coherent interferometric (CINT) imaging method which is largely based on time-reversal but exploits some of the residual coherence in the in the array measurements, in a similar way to the time-delay focusing technique.

because of the differing distances or inhomogeneities in the media but on the shape of the source. Thus causing the analysis to be inaccurate.

- The method assumes that the inhomogeneities in the medium only causes delays in the propagation of the wave front and has no effect on the spatial and temporal shape of the wave. This assumption is generally false because of refraction, diffraction and multi-scattering and in fact the assumption is only valid if inhomogeneities are small and located very close to the array of transducers.

On attempting to describe the topic of this essay to a (non-mathematically inclined and therefore long suffering) friend, their response was to ask "is that what bats do?". Bats instead use echolocation which is very similar to **SONAR** which has been well used throughout history especially for communication and military applications. Bats, whales and dolphins and many other animals make calls as they move and listen to the returning echoes to build up a map of their surroundings. How far away an object is located is deduced by how long it takes the sounds to return. They can make estimates of direction by considering the time delay between the return of the sound wave to the left and right ears. Movement of the object can be approximated by considering any changes due to the Doppler effect between the frequency of the propagated and returned wave. An intelligent and highly applicable system but requires a known sound speed and the assumption that the sound speed is homogeneous in all directions.

Moving back to **time-reversal focusing** we see how it has improved on these methods:

- The method assumes no knowledge of the background medium and the corresponding sound speed.
- The method works even if there is an inhomogeneous medium between the target and the transducers. In fact, as discussed in Section 4 we see that random media can actually enhance focusing.
- The method can deal with many types of sources that have a measurable size and may be irregular. Focusing may not be perfect but, as considered in Section 3, iterated time reversal can be used to enhance the signal to noise ratio and focus on the source.
- The method can be adapted and extended for use in the case of multiple scatterers. This is investigated further in Section 3

2.2.2 Limitations

Limitations include:

- In order for the wave equation to be symmetric in time we need to have a lossless propagation medium. Most media does not satisfy this, including biological media, for which there are many exciting applications for this method. In most cases if the attenuation coefficient in the frequency range used is sufficiently weak we are still able to use the method although over limited distances: a mouse or a human hand may be possible but an adult human torso may be too large.
- Perfect time-reversal is not possible. As discussed above: transducers have a finite size and cannot measure at all possible points. Moreover, a surface completely encircling the area of interest is almost never possible. Also as discussed by article [2] the piezoelectric transducers have a inherent natural frequency. Close to this natural frequency, resonances lead to a broadening in the temporal focusing of the time reversed wave but far from its natural frequency range we get a decrease in sensitivity and output efficiency of the transducers. Balancing these two factors is important in any experiment.

2.3 Applications

I will briefly point to just a few applications of time-reversal imaging sourced from articles [2] and [12] and Paper [15].

- **Non-Destructive testing**: Small defects are hard to find in an object with complicated geometry or made from heterogeneous materials. Moreover, testing to destruction is not possible when producing materials for practical uses. The iterative time reversal method, described in the next Section, can greatly improve the signal to noise ratio when looking for such defects and Mathias Fink's group with the French National Society for the Study and Construction of Aircraft Engines have been successful in finding defects as small as 0.4mm in a 2.5cm piece of titanium.

- **Medical Lithotripsy**: One of the major initial applications for time reversal was in the destruction of stones in kidneys and gallbladders. Ultrasonic waves are used to break up the stones but it is difficult to focus the ultrasonic waves through the changing media of the body. In addition, stones can move up to 2-3cm as the patient breathes and again when stones are broken up into smaller pieces. Using iterated time reversal, described in the next Section, the ultrasonic beam focuses tightly on the most reflective area of the stone and thus the stone can be tracked in real time.

- **Ultrasonic Medical Hyperthermia**: High-intensity ultrasound waves used to heat up and destroy tissues can be used to treat tumours in static tissues, such as a cancerous prostate gland. A patient's heart beat and breathing means that applications in other areas of the body are limited but the use of time reversal methods could go some way to make this possible.

- **Underwater Acoustics**: Wave propagation in the ocean is complex: there are multiple reflections on the rough top and bottom surfaces as well as significant disparities in wave speed in the water e.g. due to depth or salt concentration. With time reversal this scattering can be exploited to improve focusing on specific targets and improve underwater communications and imaging.

- **Thermo-acoustic and Photo-acoustic Imaging**:A short electromagnetic pulse is sent though the biological region of interest and some part of the energy is absorbed throughout the object. Absorption of energy causes thermoelastic expansion of the tissue and a pressure wave to propagate through the object which can be measured by transducers distributed around the object. The pressure at the initial moment of propagation is roughly proportional to the absorption, an important measure as, for example, cancerous cells absorb significantly more energy is the EM ranges used than healthy cells. In cases of inhomogeneous media or unknown sound speeds, time-reversal, both physical re-emission and numerical calculations can provide valuable information.

Chapter 3

Extensions of Time-Reversal

In this section we look at some extensions to the basic method, looking at the case of multiple sources or scatterers in a medium. We start, in Section 3.1 by looking at how iterative time reversal focuses on the strongest scatterer in the medium. We then move on, in section 3.2.1 to looking at methods which would allow focusing on individual scatterers in turn. Considering, only homogeneous media, in Section 3.2.2 we look at a possible method for deducing the locations of sources and some basic information on their scattering strengths.

3.1 Iterated Time reversal

3.1.1 Description

If there are several targets, the time reversal process can be iterated in order to focus on the most reflective one. Explained qualitatively in Paper [18]: we consider targets A and B of reflectivities a and b where $a > b$. [1] The first time reversed wave is made up of a sum of a wave focusing on A and one on B with amplitudes relative to the initial amplitude of a and b respectively. Repeating this n times gives a time reversed wave made of two parts, one focusing on A with relative amplitude a^n and the other focusing on B with relative amplitude b^n. For large enough n, $b^n \ll a^n$ and b^n is effectively negligible. The process has focused on the most reflective target.

Paper [13] gives some practical applications for this. In flaw detection an iterative process would help to reduce noise and focus on potential flaws. Also, in kidney stone detection the process can be used to track in real time the movement of the largest stone.

This seems to give a contradiction between the concept of iteration and time-reversal. The perfect time reversal of a perfect time reversed signal should give the original signal. The iteration would be stationary despite what we have described above. In practice time-reversal is not perfect: we might only have a finite array of transducers which don't encircle the media or we may also only measure for a finite amount of time and thus some information is lost.

3.1.2 A Quantitative Explanation

We follow and expand on the ideas in Paper [18] looking at acoustic waves and assuming that the propagation of waves is linear and that an array of N transducers is used. The analysis can be used for both inhomogeneous and homogeneous media.

We first create a response matrix $K_{lm}(t)$ (see Figure 3.1) by sending out a temporal delta function $\delta(t)$ from transducer l at location $\mathbf{y}_l$ and the returned signal is recorded at each $\mathbf{y}_m$ for $m = 1, ...N$ for a sufficiently large time scale $(0, T)$. This is done for each transducer, building up the full $N \times N$ matrix.

We can now describe what occurs if general input signals $e_m(t)$, are sent from each transducer $1 \leq m \leq N$. These propagate in the medium, reflect off scatterers and are recorded by the transducers

[1] We roughly define reflectance of a surface $R = \frac{\text{flux reflected by that surface}}{\text{flux recieved by that surface}}$

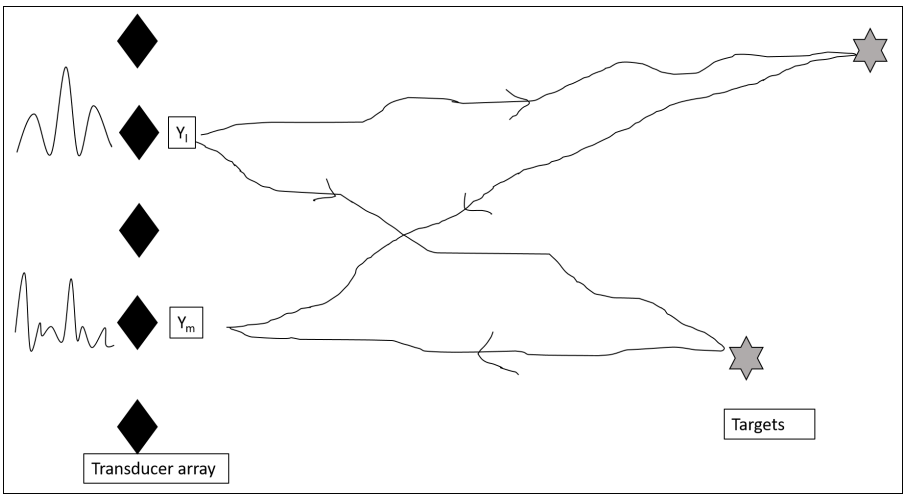

Figure 3.1: A diagram depicting the construction of the transfer matrix (also known as time reversal matrix and response matrix), K_{lm}. Inspired by a diagram in Paper [6].

$1 \leq l \leq N$ as the signal:

$$r_l(t) = \sum_{m=1}^{N} k_{lm}(t) \star_t e_m(t), \quad 1 \leq l \leq N \tag{3.1}$$

where $\star_t$ denotes a convolution in time.

A Fourier transform in time allows the convolution to be written as a multiplication:

$$R_l(\omega) = \sum_{m=1}^{N} K_{lm}(\omega) E_m(\omega), \quad 1 \leq l \leq N. \tag{3.2}$$

This allows us to consider R_l and E_m as column vectors and K_{lm} as a matrix to get

$$R(\omega) = K(\omega)E(\omega). \tag{3.3}$$

$K(\omega)$ is called the transfer matrix. We assume that due to the reciprocity theorem that the matrix K is symmetrical. Another benefit of moving into the frequency domain is that the time reversal operation is equivalent to a phase conjugation in the frequency domain[2].

We now have all the pieces to start iterating the process and consider the next lemma:

Claim - *To study multiple iterations of time reversal we should study the behaviour of the* $(K^*K)^n$

Proof. We can construct the iterative process, starting with the 0th received wave:

$$R^0 = KE^0$$

We then time reverse the received wave to get the first emitted wave

$$E^1 = K^* E^{0*}$$

and hence iterating this we get general emitted waves

$$E^{2n} = (K^*K)^n E^0 \tag{3.4}$$

$$E^{2n+1} = (K^*K)^n K^* E^{0*} \tag{3.5}$$

□

[2]e.g. for a time harmonic wave $\psi(\mathbf{x}, t) = e^{-i\omega} u(\mathbf{x})$ it is easy to see that complex conjugation is equivalent to sending $t \to -t$

We now further investigate the behaviour of $(K^*K)^n$

Lemma 3.1.1. *1. K^*K is diagonalisable with real, positive eigenvalues and orthogonal eigenvectors*

2. $E^{2n} \to \lambda_1^n V_1$ as $n \to \infty$ where λ_1 is the largest eigenvalue of K^*K and V_1 its corresponding eigenvector.

3. $E^{2n+1} \to \lambda_1^n K^* V_1^*$ as $n \to \infty$ where λ_1 is the largest eigenvalue of K^*K and V_1 its corresponding eigenvector.

In both cases we assume that $V_1 \neq 0$

Proof. We noted above that K was symmetric and thus K^*K is Hermitian. Hence, K^*K is diagonalisable with real eigenvalues and orthogonal eigenvectors.

We can show that all eigenvalues are positive by considering eigenvalue λ and corresponding eigenvector V. Then:

$$\parallel KV \parallel^2 = (KV)^\dagger (KV) = V^\dagger K^* K V = V^\dagger \lambda V = \lambda \parallel V \parallel^2 . \tag{3.6}$$

If K has $p \leq N$ distinct eigenvalues $\lambda_1 > \lambda_2 > ... > \lambda_p$ and $F_1, ..., F_p$ the corresponding eigenspaces. Let $V_i \in F_i$ and this we can write

$$E^0 = V_1 + V_2 + ... + V_p, \text{ with } V_1 \neq 0 \tag{3.7}$$

Thus using Equation 3.4 we get that:

$$E^{2n} = (K^*K)^n E^0 = \lambda_1^n V_1 + \lambda_2^n V_2 + ... + \lambda_p^n V_p \approx \lambda_1^n V_1 \tag{3.8}$$

the last approximation for large n. For an odd number of iterations we use that $K^* V_i^*$ is an eigenvector with eigenvalue λ_i:

$$(K^*K) K^* V_i^* = K^* (K^* K V_i)^* = \lambda_i K^* V_i^*. \tag{3.9}$$

Hence using Equation 3.5 we get that

$$E^{2n+1} = (K^*K)^n K^* E^{0*} = \lambda_1^n K^* V_1^* + \lambda_2^n K^* V_2^* + ... + \lambda_p^n K^* V_p^* \approx \lambda_1^n K^* V_1^* \tag{3.10}$$

again the last approximation for large n. □

Remark 2. Assuming $V_1 \neq 0$, is not a significant assumption. With some further work we find it is equivalent to the statement that says the original incident wave transmitted by the array of transducers reaches the reflector with the highest reflectivity.

Remark 3. We resolve the apparently different convergence for odd and even n by considering:

$$||K^* V_1^*||^2 = V_1^* K^* K V_1 = \lambda_1 ||V_1^*||^2 \tag{3.11}$$

and thus

$$E^{2n+1} \to \lambda_1^{n+\frac{1}{2}} e^{i\theta} V_1^* \text{ as } n \to \infty \tag{3.12}$$

which better matches the asymptotic behaviour for even values.

Remark 4. In both cases the convergence is geometrical and depends on the relative sizes of the two largest eigenvalues.

How can we interpret these eigenvalues and eigenvectors physically? We need to further investigate the transfer matrix K and so we write it as a product of three matrices which correspond to the three parts of the waves' journey:

1. A matrix describing the wave propagation from the transducers to the targets

2. A matrix describing the wave scattering off the targets

3. A matrix describing the wave propagation from the targets to the transducers

We can immediately make a two observations:

- Due to the reciprocity principle the back propagation matrix is the transpose of the forward propagation matrix
- If we assume that the targets are spaced sufficiently far apart so that there is no multiple scattering off different targets then the scattering matrix is diagonal

We consider M point-like targets with reflectivities $C_1, C_2, ..., C_M$. And define three more functions:

- $h_{il}(t)$ is the response at the location of transducer l when a temporal delta function signal is propagated from the location of scatterer i. It has Fourier transform $H_{il}(\omega)$. (Note that by the Reciprocity theorem $h_{il}(t)$ also describes the response at the location of scatterer i when a temporal delta function signal is propagated from the location of transducer l) .
- $a_e(t)$ and $a_r(t)$ are the transducers' acousto-electrical response in emission and reception with Fourier Transform $A_e(\omega)$ and $A_r(\omega)$. I include them for completeness but they could just be set to the identity.

If a signal $e_l(t)$ is propagated from each transducer, as above, the scatterer, i, receives a signal

$$p_i(t) = \sum_{l=1}^{N} e_l(t) \star_t a_e(t) \star_t h_{il}(t) \tag{3.13}$$

where in the frequency domain we can write this in matrix form

$$P = A_e H E. \tag{3.14}$$

Where P and E are vectors, H is called the diffraction matrix and is our forward propagating matrix and A_e is a constant that depends on ω.

The scattering matrix is very simple. Only considering single scattering, the pressure reflected by a scatterer only depends on the pressure received by the same scatterer. We set our scattering matrix to be $C_{ij} = \delta_{ij} C_i$ for $i, j = 1, ..., M$.

As noted above, the back propagation matrix is the transpose of the propagation matrix H. Thus taking into account the acousto-electrical response for reception we get that:

$$K = A_e A_r H^T C H \tag{3.15}$$

We confirm that is symmetrical and can now think about finding the eigenvectors and eigenvalues of $K^* K$.

If we return to our definition of $h_{il}(t)$, the signal received at l from a delta function transmitted at the location of scatterer i, then we get the signal received and processed by transducer l to be $a_r(t) \star_t h_{il}(t)$. We want to consider the case where the targets are sufficiently far apart that it is possible to focus on just one target without sending energy to the others. The best way to focus on the reflector, i, by transducer l is to time reverse the signal $a_r(t) \star_t h_{il}(t)$, the signal sent from i and recorded at l. We do this for all N transducers and get

$$P_{ji} = A_r^* A_e \sum_{l=1}^{N} H_{jl} H_{il}^*. \tag{3.16}$$

Which can be interpreted as the signal received at a target j (in the frequency domain) when a signal was emitted at the location of scatterer, i, recorded time reversed and re-emitted by all transducers and then recorded at location of scatterer j.

Which in matrix form is:

$$P_{ji} = A_r^* A_e H_j^T H_i^* \tag{3.17}$$

Where H_i is a vector with components $H_{i1}, H_{i2}, ..., H_{iN}$.

Due to the assumption that it is possible to focus on just one target we deduce that $P_{ji} \approx 0$ if $i \neq j$, hence the H_j are orthogonal. We wonder, therefore, if they might be a candidate for the eigenvectors? In fact with a little more thought, we remember that the iterative process narrows down to a wave corresponding to one single eigenvector being emitted and we wish this to focus on one scatterer. The vectors H_i^* are what would be emitted in a time reversal process if the scatterer were alone and we check that these are eigenvectors in the following lemma:

Lemma 3.1.2. *The vectors H_i^* are eigenvectors of K^*K with eigenvalues $|C_i|^2(\sum_{m=1}^{N}|H_{im}|^2)^2$. (N.B. we assume $A_e = A_r = I$)*

Proof.

$$KH_{i\,l}^* = \sum_{m=1}^{N} K_{lm}H_{im}^* = \sum_{m=1}^{N}\sum_{k=1}^{M} H_{kl}C_kH_{km}H_{im}^* \tag{3.18}$$

$$= \sum_{k=1}^{M} H_{kl}C_k \sum_{m=1}^{N} H_{km}H_{im}^* \tag{3.19}$$

$$= H_{il}C_i \sum_{m=1}^{N} |H_{im}|^2 \tag{3.20}$$

The last line following because of the orthogonality of the vectors H_i. We can see that

$$KH_i^* = C_i \sum_{m=1}^{N} |H_{im}|^2 H_i \tag{3.21}$$

$$\implies K^*KH_i^* = |C_i|^2 \left(\sum_{m=1}^{N} |H_{im}|^2\right)^2 H_i^* \tag{3.22}$$

Hence, H_i^* are indeed eigenvectors with eigenvalues $|C_i|^2(\sum_{m=1}^{N}|H_{im}|^2)^2$ □

Remark 5. We notice that the eigenvectors depend on reflectivity but also on these propagation vectors. We notice that what matters is not just the intrinsic reflectivity of the object but it's apparent reflectivity which depends on other factors such as the distance from the transducer array and the background media. It was worth doing the full proofs.

To conclude this Section, we have shown in Lemma 3.1.1 that the iterative time reversal process does indeed converge and to the eigenvector of the system with the largest eigenvalue. In Lemma 3.1.2 we showed that these eigenvectors describe a wave that focuses on a single scatterer, and the corresponding eigenvalue a function of scattering strength and other factors. We have shown that the iterative process will focus on a single scatterer.

3.2 Identification of Multiple Scatterers

Section 3.1 looks at how to efficiently focus on the most reflective scatterer but what if we needed to know about the other scatterers? For example, in Lithotripsy often multiple kidney stones exists so it would be useful if we could focus on each one in turn.

In Section 3.2.1 we qualitatively look at a common technique for this, called the DORT method, which has been used in sonar, underwater communications, non-destructive testing and medical applications (see Paper [10]).

In Section 3.2.2 we look at an extension of the DORT method, the MUSIC method, and follow Paper [10] to see how it can be expanded to estimate target scattering strengths and to cases where the targets can be closely spaced.

3.2.1 DORT Method

Paper [13] describes the DORT method. DORT is an acronym for Décomposition de l'Opérateur de Retournement Temporel , decomposition of the time reversal operator. There are three steps to the process and we have actually done most of the analysis:

1. As in Section 3.1 we compute the transfer matrix $K(w)$ by emitting a signal from each transducer in turn and measuring the response before converting to frequency space

2. We then diagonalise the operator $K^*(\omega)K(\omega)$ at a chosen frequency. If, like in Section 3.1, we assume that the scatterers are sufficiently far apart and that the number of transducers (hence the dimension of $K^*(\omega)K(\omega)$) is greater than the number of scatterers, then in most cases the number of significant eigenvalues is equal to the number of scatterers [3].

3. To find approximate locations of the scatterers we can back propagate the eigenvectors. If we have enough information about the background media this can be done numerically, else it can always be done experimentally.

It is a widely used method and a quick google scholar search will pull up multitudes of papers using this method for a wide range of applications. Restricting myself to just one example I have selected one in that, contrary to most DORT studies, the information provided by the measured array response matrix was used to avoid sending energy onto a set of scatterers instead of focusing on them. The 2009 Paper by Cochard et al. [8] looks at high intensity focused ultrasound to treat liver tumours. The ultrasound waves are focused on a precise area of cells, causing the tissue to heat up and be destroyed. However, between the liver and equipment lie the highly absorbent ribs accidental heating of the ribs can lead to severe skin burns. The ribs are the brightest scatterers in this system and hence the eigenvalues and eigenvectors corresponding to the ribs can be easily identified. The desired emission signals are then projected onto the surface orthogonal to the set of emissions that focus on the ribs. The emission should focus on the chosen point while minimising the energy that reaches the ribs. Experiments in a lab showed that this method could give a reduction by a factor of 100 of the energy reaching the ribs while retaining a similar accuracy of focusing.

3.2.2 MUSIC Method

Imaging a random media requires an ability to numerically interpret the information recorded by the array. In this Sub-section we follow paper [10] to investigate the time-reversal imaging with multiple signal classification (time-reversal MUSIC) method. We start by assuming N transceivers at positions $\mathbf{y}_k,\ k = 1, ..., N$ and M scatterers at locations $\mathbf{x}_m,\ m = 1, ..., M$. Assume $M < N$. We also assume that the transceivers are sufficiently small that they can be approximated as point elements. We also assume that we know the background Green's function G_0 of the medium i.e. that the medium is homogeneous.

We define first the 'forward' problem: consider the transceiver k emits an initial signal leading to an incident field $\psi_k^{(in)}(r, \omega)$ which interacts with the scatterers leading to a field:

$$\psi_k(\mathbf{r}, \omega) = \psi_k^{(in)}(\mathbf{r}, \omega) + \sum_{m=1}^{M} \tau_m(\omega) G_0(\mathbf{r}, \mathbf{x}_m, \omega)\psi_k(\mathbf{x}_m, \omega) \tag{3.23}$$

[3] Paper [9] notes that time-reversal matrix for N element array embedded in a three-dimensional homogeneous background and containing $1 < M \leq N$ targets will have rank $< M$ if and only if the following conditions hold:

(a) All of the targets are located on a single plane P that is orthogonal to at least $N - M + 1$ lines $l_{j,l}$ connecting different transducer elements labelled by indices j and l,

(b) The plane P is the perpendicular bisector of the $N - M + 1$ lines satisfying condition (1) or all targets on P are equidistant from every line satisfying condition (1).

This is unlikely to ever occur in any practical application and hence we can safely ignore it. However, it is nice to note for completeness

where $\tau_m(\omega)$ is a measure of the reflectivity of the m^{th} scatterer. If we knew what these scattering strengths are, and the values of the incident field at the points x_m (assuming we know these locations), then we would be able to evaluate the field at an arbitrary point as long as we knew the values of the $\psi_k(\mathbf{x}_m, \omega)$. We are tempted to set $\mathbf{r} = \mathbf{x}_m$ to see if this would give us any more information. This is a good idea up to the point we realise that $G(\mathbf{x}_m, \mathbf{x}_m, \omega)$ is singular.

We resolve this by interpreting $G(\mathbf{x}_m, \mathbf{x}_m, \omega)$ as instead a 'self-field' contribution caused by interactions within the scatterer which can absorbed into the definitions of the scattering strengths. We can thus safely ignore the $G(\mathbf{x}_m, \mathbf{x}_m, \omega)$ term and the possible singularities. We then get the Foldy-Lax equations:

$$\psi_k(\mathbf{x}_m, \omega) = \psi_k^{(in)}(\mathbf{x}_m, \omega) + \sum_{m \neq m'} \tau_{m'}(\omega) G_0(\mathbf{x}_m, \mathbf{x}_{m'}, \omega) \psi_k(\mathbf{x}_{m'}, \omega) \tag{3.24}$$

which can be written in matrix form:

$$H\Psi_k = \Psi_k^{\text{in}}. \tag{3.25}$$

Where:

$$\Psi_k = [\psi_k(\mathbf{x}_1, \omega), \psi_k(\mathbf{x}_2, \omega), ..., \psi_k(\mathbf{x}_M, \omega)]^T \tag{3.26}$$

$$\Psi_k^{\text{in}} = [\psi_k^{\text{in}}(\mathbf{x}_1, \omega), \psi_k^{\text{in}}(\mathbf{x}_2, \omega), ..., \psi_k^{\text{in}}(\mathbf{x}_M, \omega)]^T \tag{3.27}$$

$$H_{m,m'} = \delta_{m,m'} - (1 - \delta_{m,m'}) \tau_{m'}(\omega) G_0(\mathbf{x}_m, \mathbf{x}_{m'}, \omega). \tag{3.28}$$

H is symmetric and in almost all cases will have a unique inverse.

The inverse problem is that given the value of the field can we find both the target positions x_m and the scattering strengths τ_m?

At the moment, this seems impenetrable and so we look again at equations 3.23 and 3.24 and see if we can get any further. We assumed that the transceivers are point like and hence if the k^{th} transceiver emits a temporal delta function then $\psi_k^{(\text{in})}(\mathbf{r}, \omega)$ is the background Green's function $G_0(\mathbf{r}, \mathbf{x}_k, \omega)$ and $\psi_k(\mathbf{r}, \omega)$ is the full Green's function for the whole system $G(\mathbf{r}, \mathbf{x}_k, \omega)$. We reformulate equations 3.23 and 3.24 to get:

$$G(\mathbf{r}, \mathbf{y}_k, \omega) = G_0(\mathbf{r}, \mathbf{y}_k, \omega) + \sum_{m=1}^{M} \tau_m(\omega) G_0(\mathbf{r}, \mathbf{x}_m, \omega) G(\mathbf{x}_m, \mathbf{y}_k, \omega) \tag{3.29}$$

$$G(\mathbf{x}_m, \mathbf{y}_k \omega) = G_0(\mathbf{x}_m, \mathbf{y}_k, \omega) + \sum_{m \neq m'} \tau_{m'}(\omega) G_0(\mathbf{x}_m, \mathbf{x}_{m'}, \omega) G(\mathbf{x}_{m'}, \mathbf{y}_k, \omega) \tag{3.30}$$

We need more information to continue. Considering the values of the system that we can measure we think back to Section 3.1 and diagram 3.1 and the time reversal matrix K:

$$K_{j,k} = G(\mathbf{y}_j, \mathbf{y}_k, \omega) - G_0(\mathbf{y}_j, \mathbf{y}_k, \omega) \tag{3.31}$$

$$= \sum_{m=1}^{M} \tau_m(\omega) G_0(\mathbf{x}_j, \mathbf{y}_m, \omega) G(\mathbf{x}_m, \mathbf{y}_k, \omega) \tag{3.32}$$

$$= \sum_{m=1}^{M} \tau_m(\omega) G_0(\mathbf{x}_m, \mathbf{y}_j, \omega) G(\mathbf{x}_m, \mathbf{y}_k, \omega) \tag{3.33}$$

where we have used Equation 3.29 and the the standard reciprocity conditions (the position of the point source and the observer can be reversed, as described in Paper [11]). Using Equation 3.31 and reciprocity also gives that K is symmetric and we breathe a sigh of relief.

Now for the huge assumption that if the targets are 'well resolved' and thus there is no multiple scattering between targets and thus:

$$G(\mathbf{r}, \mathbf{x}_m, \omega) \approx G_0(\mathbf{r}, \mathbf{x}_m, \omega). \tag{3.34}$$

Hence, that after the wave has interacted with the scatterer $\mathbf{x}_m$ it is no longer going to interact with any other scatterer and we can model its propagation using only the background Green's function, we don't need information about any other scatterer. This then gives:

$$\implies K_{j,k} \approx K^b_{j,k} := \sum_{m=1}^{M} \tau_m(\omega) G_0(\mathbf{x}_m, \mathbf{y}_j, \omega) G_0(\mathbf{x}_m, \mathbf{y}_k, \omega) \tag{3.35}$$

$$\implies K = \sum_{m=1}^{M} \tau_m(\omega) g_0(\mathbf{x}_m, \omega) g_0^T(\mathbf{x}_m, \omega) \tag{3.36}$$

$$\text{where} \quad g_0(\mathbf{x}_m, \omega) = [G_0(\mathbf{x}_m, \mathbf{y}_1, \omega), G_0(\mathbf{x}_m, \mathbf{y}_2, \omega), ..., G_0(\mathbf{x}_m, \mathbf{y}_N, \omega)]. \tag{3.37}$$

With this assumption we have all the pieces we need to compute the locations and reflectivity of scatterers.

3.2.2.1 Computing location of the scatterers

Lemma 3.2.1. *There exists a function $\Phi(\boldsymbol{x})$ with singular peaks only at $\boldsymbol{x} = \boldsymbol{x}_m, m = 1, ..., M$, the locations of the scatterers*

Proof. We consider a singular value decomposition of K. Defining:

- The N orthonormal eigenvectors of $K^\dagger K$ to be v_p
- The N orthonormal eigenvectors of $KK^\dagger$ to be u_p
- The square root of the eigenvalues of $K^\dagger K$ and $KK^\dagger$ are σ_p

Hence,

$$Kv_p = \sigma_p u_p \quad \text{and} \quad K^\dagger u_p = \sigma_p v_p \tag{3.38}$$

$$\text{thus } K = \sum_{p=1}^{N} \sigma_p u_p v_p^\dagger \tag{3.39}$$

We now have two different descriptions of K, Equation 3.36 and 3.39 and we hope to link the two. We see that the matrix K maps C^N to $S_0 = \text{Span}\{g_0(\mathbf{x}_m, \omega), m = 1, ..., M\}$ and also $S_0 = \text{Span}\{u_p | \sigma_p > 0\} \perp N_0 := \text{Span}\{u_p | \sigma_p = 0\ \}$. With $S_0 \perp N_0$ following because the u_p are orthonormal eigenvectors.

Hence, if $\sigma_q = 0$ then u_q is perpendicular to all vectors in S_0 and hence[4]:

$$u_q^\dagger g_0(\mathbf{x}_m, \omega) = 0, \quad \forall m = 1, ..., M. \tag{3.40}$$

The converse follows similarly: if $u_q^\dagger g_0(\mathbf{x}, \omega) = 0$ for all q such that $\sigma_q = 0$ then $g_0(\mathbf{x}, \omega) \in N_0^\perp = S_0$. Hence $g_0(\mathbf{x}, \omega) \in \text{Span}\{g_0(\mathbf{x}_m, \omega), m = 1, ..., M\}$. Thus $\mathbf{x} = \mathbf{x}_m$ for some $m = 1, ..., M$.

Hence we define a function:

$$\Phi(\mathbf{x}) = \frac{1}{\sum_{\sigma_q = 0} |u_q^\dagger g_0(\mathbf{x}, \omega)|^2} \tag{3.41}$$

Which should have singular peaks only at $\mathbf{x} = \mathbf{x}_m, m = 1, ..., M$ and hence we can find approximate locations for the reflectors.

□

Remark 6. $\Phi(\mathbf{x})$ is called the 'time-reversal MUSIC pseudo-spectrum.'

Remark 7. Given that K is symmetric, we could repeat this analysis with K^T and get the function $\Phi(\mathbf{x}) = \dfrac{1}{\sum_{\sigma_q = 0} |v_q^\dagger g_0^*(\mathbf{x}, \omega)|^2}$

Remark 8. $\Phi(\mathbf{x})$ is one of many such functions that could work but I suggest some reasoning behind the choice:

[4]N.B it could be the case that $N_0 = \emptyset$. It can be shown, although we will not do it here, that this is the case only if $M \geq N$. Hence the requirement that $N < M$. Qualitatively, this requirement is expected as you feel like you should have more knowns than unknowns.

- the absolute value of $u_q^\dagger g_0(\mathbf{x}_m, \omega)$ has been chosen to simplify the programming challenge to just finding large positive peaks and not needing to look for large negative peaks as well
- the square of $|u_q^\dagger g_0(\mathbf{x}_m, \omega)|$ is taken to increase the gap between actually singular values and the rest of the noise
- the sum over the set $Q = \{q|\sigma_q = 0\}$ is taken because $u_q^\dagger g_0(\mathbf{x}_m, \omega) = 0, \quad \forall q \in Q$. It could be possible that by chance for some $\mathbf{x}$ and some $q \in Q$ that $u_q^\dagger g_0(\mathbf{x}_m, \omega) \approx 0$ but it is unlikely that this is true for all $q \in Q$

3.2.2.2 Computing the the scattering strengths of the targets

We return to Equation 3.36 and realise that as we now have estimates for the positions $\mathbf{x}_m$ we can now compute $G_0(\mathbf{x}_m, \mathbf{y}_j, \omega)G_0(\mathbf{x}_m, \mathbf{y}_k, \omega)$ and the only unknown left in the Equation is $\tau_m(\omega)$. Thus we can solve to find these values for example by writing:

- $[K_{j,k}] = [K_{1,1}, K_{1,2}..., K_{1,N}, K_{2,1}, K_{2,2}, ..., K_{N,N}]^T$ a $N^2 \times 1$ vector
- $[\tau_m(\omega)] = [\tau_N(\omega), ..., \tau_M(\omega)]^T$ a $M \times 1$ vector
- $[G_0(\mathbf{x}_m, \mathbf{y}_j, \omega)G_0(\mathbf{x}_m, \mathbf{y}_k, \omega)] =$
$$\begin{bmatrix} G_0(\mathbf{x}_1, \mathbf{y}_1, \omega)G_0(\mathbf{x}_1, \mathbf{y}_1, \omega) & \cdots & G_0(\mathbf{x}_M, \mathbf{y}_1, \omega)G_0(\mathbf{x}_M, \mathbf{y}_1, \omega) \\ G_0(\mathbf{x}_1, \mathbf{y}_1, \omega)G_0(\mathbf{x}_1, \mathbf{y}_2, \omega) & \cdots & G_0(\mathbf{x}_M, \mathbf{y}_1, \omega)G_0(\mathbf{x}_M, \mathbf{y}_2, \omega) \\ \vdots & \vdots & \vdots \\ G_0(\mathbf{x}_1, \mathbf{y}_N, \omega)G_0(\mathbf{x}_1, \mathbf{y}_N, \omega) & \cdots & G_0(\mathbf{x}_M, \mathbf{y}_N, \omega)G_0(\mathbf{x}_M, \mathbf{y}_N, \omega) \end{bmatrix}, \text{ a } N^2 \times M \text{ matrix}$$

This gives:

$$[K_{j,k}] = [G_0(\mathbf{x}_m, \mathbf{y}_j, \omega)G_0(\mathbf{x}_m, \mathbf{y}_k, \omega)][\tau_m(\omega)] \tag{3.42}$$

which can be solved, e.g. by the least squares method.

3.2.2.3 In the presence of multiple scattering

For multiple scattering, we can't make the assumption that $G(\mathbf{x}_m, \mathbf{y}_k, \omega) \approx G_0(\mathbf{x}_m, \mathbf{y}_k, \omega)$ so instead we go back to Equation 3.33 and write:

$$KK^b = \sum_{m=1}^{M} \tau_m(\omega) g_0(\mathbf{x}_m, \omega) g^T(\mathbf{x}_m, \omega) \tag{3.43}$$

$$\text{where} \quad g(\mathbf{x}_m, \omega) = [G(\mathbf{x}_m, \mathbf{y}_1, \omega), G(\mathbf{x}_m, \mathbf{y}_2, \omega), ..., G(\mathbf{x}_m, \mathbf{y}_N, \omega)] \tag{3.44}$$

We follow the same process as above and get two time-reversal MUSIC psuedospectra:

$$\Phi_1(\mathbf{x}) = \frac{1}{\sum_{\sigma_q=0} |u_q^\dagger g_0(\mathbf{x}, \omega)|^2} \tag{3.45}$$

$$\Phi_2(\mathbf{x}) = \frac{1}{\sum_{\sigma_q=0} |v_q^\dagger g^*(\mathbf{x}, \omega)|^2} \tag{3.46}$$

where miraculously $\Phi_1(\mathbf{x})$ is the same function as we had previously! We can use this Equation to estimate the locations of scatterers even if we do not know how far apart the scatterers are and only with the background Green's function.

To find scattering strengths, consider the same method as above:

- $[K_{j,k}] = [K_{1,1}, K_{1,2}..., K_{1,N}, K_{2,1}, K_{2,2}, ..., K_{N,N}]^T$ a $N^2 \times 1$ vector
- $[\tau_m(\omega)] = [\tau_1(\omega), ..., \tau_M(\omega)]^T$ a $M \times 1$ vector

- $[G_0(\mathbf{x}_m, \mathbf{y}_j, \omega)G(\mathbf{x}_m, \mathbf{y}_k, \omega)] =$
$$\begin{bmatrix} G_0(\mathbf{x}_1, \mathbf{y}_1, \omega)G(\mathbf{x}_1, \mathbf{y}_1, \omega) & \cdots & G_0(\mathbf{x}_M, \mathbf{y}_1, \omega)G(\mathbf{x}_M, \mathbf{y}_1, \omega) \\ G_0(\mathbf{x}_1, \mathbf{y}_1, \omega)G(\mathbf{x}_1, \mathbf{y}_2, \omega) & \cdots & G_0(\mathbf{x}_1, \mathbf{y}_1, \omega)G(\mathbf{x}_M, \mathbf{y}_2, \omega) \\ \vdots & \vdots & \vdots \\ G_0(\mathbf{x}_1, \mathbf{y}_N, \omega)G(\mathbf{x}_1, \mathbf{y}_N, \omega) & \cdots & G_0(\mathbf{x}_M, \mathbf{y}_N, \omega)G(\mathbf{x}_M, \mathbf{y}_N, \omega) \end{bmatrix}, \text{ a } N^2 \times M \text{ matrix}$$

Giving:

$$[K_{j,k}] = [G_0(\mathbf{x}_m, \mathbf{y}_j, \omega)G(\mathbf{x}_m, \mathbf{y}_k, \omega)][\tau_m(\omega)] \tag{3.47}$$

A much more difficult problem than we solved for the single scattering case. The full Green's function, G, is still unknown giving us two sets of unknowns in the Equation. The equations are also not linear in these unknowns containing products of the Green's functions and the scattering strengths. We can no longer use the least squares method.

Returning the Foldy-Lax formulation we can find another set of equations linking G, G_0 and τ_i, we consider Equation 3.25 setting:

$$\Psi_k = [G(\mathbf{x}_1, \mathbf{y}_k, \omega), G(\mathbf{x}_2, \mathbf{y}_k, \omega), ..., G(\mathbf{x}_m, \mathbf{y}_k, \omega)]^T = [G(\mathbf{x}_m, \mathbf{y}_k, \omega)] \tag{3.48}$$
$$\Psi_k = [G_0(\mathbf{x}_1, \mathbf{y}_k, \omega), G_0(\mathbf{x}_2, \mathbf{y}_k, \omega), ..., G_0(\mathbf{x}_m, \mathbf{y}_k, \omega)] = [G_0(\mathbf{x}_m, \mathbf{y}_k, \omega)]^T \tag{3.49}$$

and recalling:

$$H_{m,m'} = \delta_{m,m'} - (1 - \delta_{m,m'})\tau_{m'}(\omega)G_0(\mathbf{x}_m, \mathbf{x}_{m'}, \omega) \tag{3.50}$$

we get the Equation

$$H[G(\mathbf{x}_m, \mathbf{y}_k, \omega)] = [G_0(\mathbf{x}_m, \mathbf{y}_k, \omega)], \quad k = 1, 2, ..., N. \tag{3.51}$$

Combining equations 3.51 and 3.47 Paper [10] describes one possible iteration scheme to estimate the scattering strengths and the full Green's functions:

$$[K_{j,k}] = [G_0(\mathbf{x}_m, \mathbf{y}_j, \omega)G^{(n)}(\mathbf{x}_m, \mathbf{y}_k, \omega)][\tau_m^{(n+1)}(\omega)] \tag{3.52}$$
$$H^{(n+1)} = \delta_{m,m'} - (1 - \delta_{m,m'})\tau_{m'}^{(n+1)}(\omega)G_0(\mathbf{x}_m, \mathbf{x}_{m'}, \omega) \tag{3.53}$$
$$H^{(n+1)}[G^{(n+1)}(\mathbf{x}_m, \mathbf{y}_k, \omega)] = [G_0(\mathbf{x}_m, \mathbf{y}_k, \omega)] \tag{3.54}$$

The initial value for $G^{(0)}$ is taken as $G^{(0)} = G_0$. This is equivalent to the assumption that there is no multi-scattering and hence and $\tau_m^{(1)}$, obtained by Equation 3.52, is the predicted scattering strengths we saw in the previous section under the no multi-scattering assumption (see Equation 3.42). $H^{(1)}$ is then deduced by Equation 3.53 and then $G^{(1)}$ by Equation 3.54. The process is then iterated and we can see that a fixed point of this iteration system is the required solution.

It works in some cases but unfortunately added noise or closely clustered targets can cause convergence problems.

3.3 Summary

In this Section, I have described just a small selection of possible extensions and applications of time reversal. I have considered cases where there are multiple scatterers and how iterated time reversal allows you to focus on the strongest scatterer. The DORT and the MUSIC method uses properties of the transfer matrix K, which can be constructed, as described in Figure 3.1, to focus on individual scatters or for imaging purposes, where we want to numerically back-propagate the wave. For the MUSIC method, we mainly considered single scattering in a homogeneous medium and briefly looked at multiple scattering. To consider inhomogeneous media, it first requires some investigation on the statistical stability of time reversal, so we will return to this in Section 4.3.

Chapter 4

'Super Resolution' in Random media

As hinted previously, experimental results show that focusing improves due to the effects of a random medium, a counter-intuitive phenomena that I will attempt to explain in this Section

We assume an array of N transducers located at $\mathbf{x}_p$ for $p = 1, ..., N$ and an unknown media containing $M < N$ scatterers at locations $\mathbf{y}_p$. Two adjacent transducers are a distance $\lambda/2$ apart, where λ is the central wavelength of the pulses emitted by the transducers. Transducers behave like an array of length $a = (N-1)\lambda/2$ and interference between transducers is minimised. We take the distance between the array and the scatterers to be of length L. An example of the set-up for oa single reflector is seen in Figure 4a.

We choose the media to be randomly inhomogeneous with l the correlation length of the random fluctuations. For the purpose of this Section we make these assumptions:

1. The length of the array is relatively small so that the random-media has an effect i.e. $a \ll L$.
2. That $\lambda \lessapprox l \ll a \ll L$: the correlation length, l, of the inhomogeneities is small ad the wave Lenten, λ, is short compared to the correlation length
3. The random fluctuations are weak (a standard deviation of 5% or less) so that waves are mostly scattered in the forward direction
4. The targets are large enough or reflective enough that they stand out from the background scatterers.

4.1 'Super Resolution'

4.1.1 Qualitative description

Qualitatively we find that random homogeneities in the medium cause information that would previously not be detected by the array to be reflected onto the array and thus the array appears to have a larger aperture a_e which is larger than a, the actual physical size. An example of this can be seen in Figure 4c line i. We call this phenomena multipathing. Further thought also suggests that multipathing will also scatter some of the signals away from the array that would previously have hit the array e.g. line ii in Figure 4c. This causes a reduction in the intensity of the signal but, as Paper [6] suggests, linearity of the wave equation allows us to simply amplify the signal meaning this has no great effect.

An alternative explanation[1], described in Lectures [19], considers that in a high frequency domain then we can view the waves as rays and utilise ray theory. The idea is that for the back propagated wave, interference from multiple paths is constructive at the source location: the phase shift caused by multiple scattering is exactly compensated when the time-reversed signal follows the same path back to the source. Everywhere else however, the interference is destructive: the phase shift along other paths just averages out.

[1]For a more detailed investigation of this line of enquiry see Paper [21]

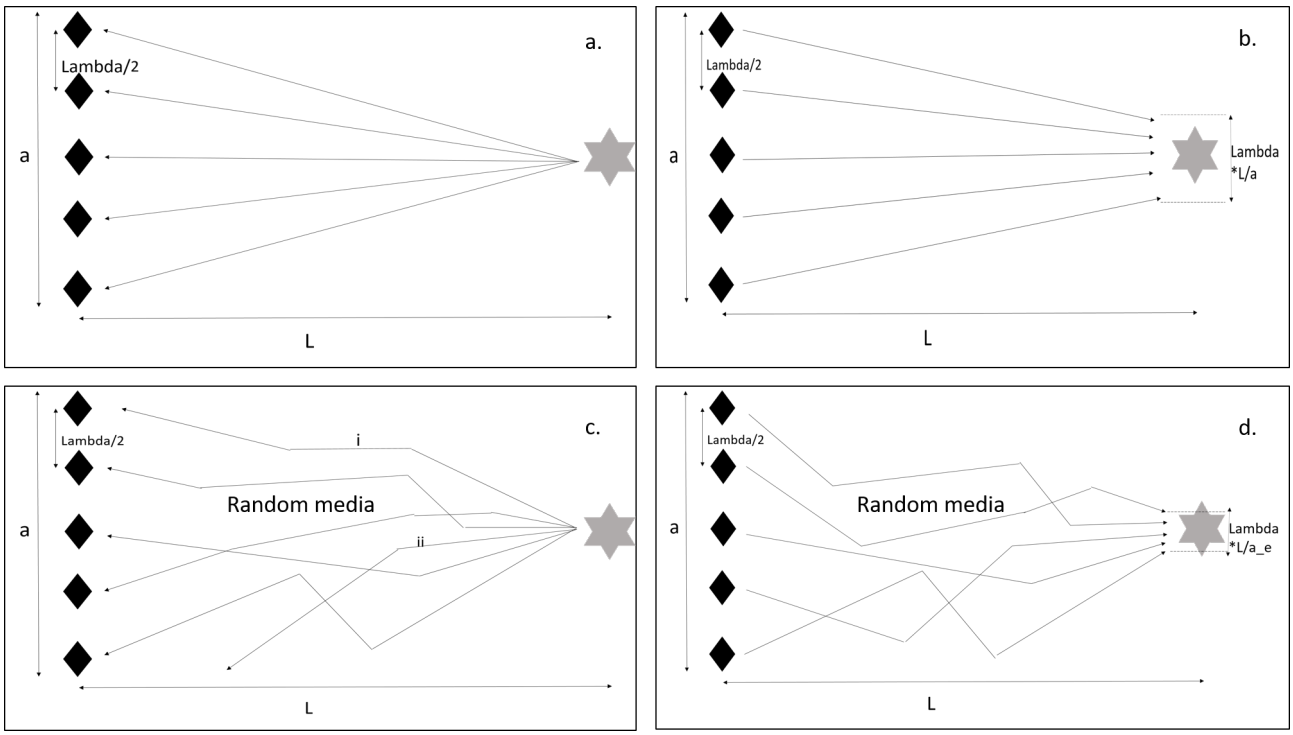

Figure 4.1: Time reversal in homogeneous media (a and b) and inhomogeneous media (c and d). The focusing is tighter in the inhomogeneous media due to multipathing. Diagrams inspired by those in Paper [6]

These are both very 'hand-wavy' explanations and leave us unsatisfied so we look at how to explain this with more mathematical rigour.

4.1.2 Quantitative Analysis

In this Section we look at the case where $M = 1$, only one scatterer, and show that for homogeneous media the back propagated field has a cross range resolution of approximately $\lambda L/a$, where for inhomogeneous media we get a width of $\lambda L/a_e$, where $a_e > a$ and a case of 'Super Resolution'. We follow the work of Paper [4] to show that this effective aperture for a array with a Gaussian aperture is

$$a_e = a\sqrt{1 + \frac{L^3\gamma}{a^2}} > a \tag{4.1}$$

where γ is a constant that depends on the statistics of the random fluctuations. Also we will show that for a finite aperture the effective aperture satisfies $a_e > a$.

Throughout this Section we define the Fourier transform to be:

$$\hat{f}(p) = \frac{1}{(2\pi)^d}\int_{R^d} e^{ip\cdot x} f(x)dx \tag{4.2}$$

$$f(x) = \int_{R^d} e^{-ip\cdot x}\hat{f}(p)dp, \tag{4.3}$$

4.1.2.1 Defining the back-propagated wave

We start by following the Paper [4]. We first aim to define the back-propagated wave under the assumptions above. We consider a a set of transducers placed in the plane $z = L$ covering a region A which can be described by the indicator function:

$$\chi_A(\mathbf{y}) = \begin{cases} 1, \text{ if } \mathbf{y} \in A \\ 0, \text{ if } \mathbf{y} \notin A \end{cases} \tag{4.4}$$

We first aim to define the back-propagated wave:

Lemma 4.1.1. *Consider an initial emitted wave to be a Gaussian beam in the frequency domain, described at $z_0 = 0$ by $\psi_0(\eta; k)$. This propagates in the medium and is reflected by transducers at locations covering a region A, in the plane $z = L$. The back-propagated can be described by:*

$$\psi^B(\xi, L; k) = \int\int \chi_A(\boldsymbol{y})\overline{\psi_0(\eta, k)}\Gamma(L, \boldsymbol{y}, \boldsymbol{y}; \xi, \eta; k)d\eta \; d\boldsymbol{y} \tag{4.5}$$

Where Γ is defined as:

$$\Gamma(L, \boldsymbol{x}, \boldsymbol{y}; \xi, \eta; k) = G(L, 0; \boldsymbol{x}, \xi; k)\overline{G(L, 0; \boldsymbol{y}, \eta; k)} \tag{4.6}$$

$$\implies \Gamma(0, \boldsymbol{x}, \boldsymbol{y}; \xi, \eta; k) = \delta(\boldsymbol{x} - \xi)\delta(\boldsymbol{y} - \eta) \tag{4.7}$$

and G is a Green's function.

Proof. We consider only time-harmonic waves $e^{-i\omega t}u(x, y, z)$. They also satisfy the Helmholtz Equation:

$$u_{xx} + u_{yy} + u_{zz} + k^2n^2(x, y, z) = 0 \text{ where } \frac{\omega}{c_0} = k \text{ and } n(x, y, z) = c_0/c(x, y, z) \tag{4.8}$$

defining c is the propagation speed and c_0 is a reference speed. We note also note that reversing time (ie sending $t \to -t$) is the same as taking complex conjugates. Weak inhomogeneities imply that, away from the point source, we can use the parabolic or paraxial approximation[2]. We consider the wave propagating mainly in the z-direction and hence of the form $u = e^{ikz}\psi(x, y, z)$. This reduces the wave Equation to a Schrödinger Equation with z playing the role of time:

$$2ik\psi_z + \nabla_\perp\psi + k^2(n^2 - 1)\psi = 0, \text{ where } \psi|_{z=0} = \psi_0(\mathbf{x}; k), \quad \mathbf{x} = (x, y), \text{ and } \nabla_\perp\psi = \psi_{xx} + \psi_{yy} \tag{4.9}$$

It makes sense to now define a Green's function and we consider a point source at (z_0, ξ) where $\xi = (x_0, y_0)$ and the Green's function $G(z, z_0; \mathbf{x}, \xi; k)$.

A few points follow immediately:

- It must also satisfy the parabolic Equation :

$$2ikG_z + \Delta_{\mathbf{x}}G + k^2\mu(\mathbf{x}, z)G = 0, \tag{4.10}$$

  where $G(z_0, z_0; \mathbf{x}, \xi; k) = \delta(\mathbf{x} - \xi), \; z > z_0$ and $\mu(\mathbf{x}, z) = n^2(\mathbf{x}, z) - 1$.

- Reciprocity implies

$$G(z, z_0; \mathbf{x}, \xi; k) = G(z_0, z; \xi, \mathbf{x}; k). \tag{4.11}$$

- By definition of the Green's function we have that the wave field at $z = L$ is given by:

$$\psi(\mathbf{y}, L; k) = \int G(L, 0; \mathbf{y}, \eta; k)\psi_0(\eta, k) \; d\eta. \tag{4.12}$$

This gives us the forward propagating wave.

Transducers at points in region A then time reverse the wave, which is equivalent to complex conjugation. So we consider a new initial value problem with source wave $\overline{\psi(\mathbf{y}, L; k)}\chi_A(\mathbf{y})$. We can now express the value of the back-propagated wave in the plane $z = 0$ at the point $\xi = (x, y)$ as:

$$\psi^B(\xi, L; k) = \int G(0, L; \xi, \mathbf{y}; k)\overline{\psi(\mathbf{y}, L; k)}\chi_A(\mathbf{y})d\mathbf{y}. \tag{4.13}$$

[2]See any course in wave scattering, including [19]. The idea is that if we suppose ψ is propagating at a small angle to the horizontal, i.e. in 2-D, $\psi(x, z) = e^{ik(x\cos(\alpha)+z\sin(\alpha))}$ where α is small. The fastest variation of ψ is done close to the x-direction, so define the 'slowly varying part' E of ψ by $E = \psi e^{-ikx}$. Substituting this into the Helmholtz Equation will give a Schrödinger-like Equation

We recall reciprocity to get:

$$\psi^B(\xi, L; k) = \int G(L, 0; \mathbf{y}, \xi; k)\overline{\psi(\mathbf{y}, L; k)}\chi_A(\mathbf{y})d\mathbf{y} \tag{4.14}$$

Now include the formula for the forward wave from Equation 4.12:

$$\psi^B(\xi, L; k) = \int\int \overline{G(L, 0; \mathbf{y}, \eta; k)\psi_0(\eta, k)}d\eta\ G(L, 0; \mathbf{y}, \xi; k)\chi_A(\mathbf{y})d\mathbf{y} \tag{4.15}$$

$$= \int\int \chi_A(\mathbf{y})\overline{\psi_0(\eta, k)}\Gamma(L, \mathbf{y}, \mathbf{y}; \xi, \eta; k)d\eta\ d\mathbf{y} \tag{4.16}$$

□

Remark 9. $\Gamma(L, \mathbf{y}, \mathbf{y}; \xi, \eta; k)$ can be interpreted as the final response at the source plane ($z = 0$) as a result of a point source at η, whose signal is recorded by a transducer at $\mathbf{y}$, time reversed back-propagated and observed at ξ. This appears to be a crucial term and so we investigate further.

4.1.2.2 Investigating the function Γ

We want to investigate the function $\Gamma(L, \mathbf{x}, \mathbf{y}; \xi, \eta; k)$ and so we look to the only piece of information about G that we noted but haven't used yet: $G(z, z_0; \mathbf{x}, \xi; k)$ satisfies Equation 4.10. This leads to the following lemma:

Lemma 4.1.2. $\Gamma(L, \boldsymbol{x}, \boldsymbol{y}; \xi, \eta; k)$ *satisfies*

$$2ik\frac{\partial\Gamma}{\partial L} + (\Delta_{\boldsymbol{x}} - \Delta_{\boldsymbol{y}})\Gamma + k^2(\mu(\boldsymbol{x}, L) - \mu(\boldsymbol{y}, L))\Gamma = 0 \tag{4.17}$$

with initial conditions

$$\Gamma(0, \boldsymbol{x}, \boldsymbol{y}; \xi, \eta; k) = \delta(\boldsymbol{x} - \xi)\delta(\boldsymbol{y} - \eta). \tag{4.18}$$

Proof. We recall Equation 4.10:

$$2ikG_z + \Delta_{\mathbf{x}}G + k^2\mu(\mathbf{x}, z)G = 0 \tag{4.19}$$

$$\implies 2ik\bar{G}_z - \Delta_{\mathbf{x}}\bar{G} - k^2\mu(\mathbf{x}, z)\bar{G} = 0. \tag{4.20}$$

By multiplying by relevant factors of G or $\bar{G}$ we get

$$2ik\overline{G(L, 0; \mathbf{y}, \eta; k)}\frac{\partial G(L, 0; \mathbf{x}, \xi; k)}{\partial L} + \overline{G(L, 0; \mathbf{y}, \eta; k)}\Delta_{\mathbf{x}}G(L, 0; \mathbf{x}, \xi; k)$$
$$+ k^2\mu(\mathbf{x}, L)\overline{G(L, 0; \mathbf{y}, \eta; k)}G(L, 0; \mathbf{x}, \xi; k) = 0 \tag{4.21}$$

and

$$2ikG(L, 0; \mathbf{x}, \xi; k)\frac{\partial\overline{G(L, 0; \mathbf{y}, \eta; k)}}{\partial L} - G(L, 0; \mathbf{x}, \xi; k)\Delta_{\mathbf{y}}\overline{G(L, 0; \mathbf{y}, \eta; k)}$$
$$- k^2\mu(\mathbf{y}, L)G(L, 0; \mathbf{x}, \xi; k)\overline{G(L, 0; \mathbf{y}, \eta; k)} = 0. \tag{4.22}$$

Adding Equation 4.21 and Equation 4.22 we derive an Equation for $\Gamma(L, \mathbf{x}, \mathbf{y}; \xi, \eta; k)$ given by:

$$2ik\frac{\partial\Gamma}{\partial L} + (\Delta_{\mathbf{x}} - \Delta_{\mathbf{y}})\Gamma + k^2(\mu(\mathbf{x}, L) - \mu(\mathbf{y}, L))\Gamma = 0. \tag{4.23}$$

Initial conditions are easily obtained from the definition of Γ and G:

$$\Gamma(0, \mathbf{x}, \mathbf{y}; \xi, \eta; k) = \delta(\mathbf{x} - \xi)\delta(\mathbf{y} - \eta). \tag{4.24}$$

□

We now change variables in the transverse plane, which will make sense later on:

$$\mathbf{X} = \frac{\mathbf{x}+\mathbf{y}}{2},\ \mathbf{Y} = \frac{\mathbf{y}-\mathbf{x}}{2} \tag{4.25}$$

$$\implies \mathbf{x} = \mathbf{X} - \frac{\mathbf{Y}}{2},\ \mathbf{y} = \mathbf{X} + \frac{\mathbf{Y}}{2} \tag{4.26}$$

$$\implies (\Delta_{\mathbf{x}} - \Delta_{\mathbf{y}}) = (\nabla_{\mathbf{x}} - \nabla_{\mathbf{y}})(\nabla_{\mathbf{x}} + \nabla_{\mathbf{y}}) = -2\nabla_{\mathbf{X}}\nabla_{\mathbf{Y}} \tag{4.27}$$

Thus we can rewrite equations 4.17 and 4.18 to get:

$$2ik\frac{\partial \Gamma}{\partial L} - 2\nabla_{\mathbf{X}}\nabla_{\mathbf{Y}}\Gamma + k^2(\mu(\mathbf{X} - \frac{\mathbf{Y}}{2}, L) - \mu(\mathbf{X} + \frac{\mathbf{Y}}{2}, L))\Gamma = 0 \tag{4.28}$$

$$\Gamma(0, \mathbf{X}, \mathbf{Y}; \xi, \eta; k) = \delta(\mathbf{X} - \frac{\mathbf{Y}}{2} - \xi)\delta(\mathbf{X} + \frac{\mathbf{Y}}{2} - \eta) \tag{4.29}$$

We now introduce the **Wigner transform**[3] **of** Γ: in our case the Fourier transform of Γ in the $\mathbf{Y}$ direction:

$$W(L, \mathbf{X}, \mathbf{P}, \xi, \eta; k) = \frac{1}{(2\pi)^d}\int e^{i\mathbf{P}\cdot\mathbf{Y}}\Gamma(L, \mathbf{X}, \mathbf{Y}; \xi, \eta; k)d\mathbf{Y}. \tag{4.30}$$

We thus Fourier transform equations 4.28 and 4.29 to get:

$$\frac{1}{(2\pi)^d}\int e^{i\mathbf{P}\cdot\mathbf{Y}}2ik\frac{\partial\Gamma}{\partial L}d\mathbf{Y} - \frac{1}{(2\pi)^d}\int e^{i\mathbf{P}\cdot\mathbf{Y}}2\nabla_{\mathbf{X}}\nabla_{\mathbf{Y}}\Gamma d\mathbf{Y} + \frac{1}{(2\pi)^d}\int e^{i\mathbf{P}\cdot\mathbf{Y}}k^2\left(\mu\left(\mathbf{X} - \frac{\mathbf{Y}}{2}, L\right) - \mu\left(\mathbf{X} + \frac{\mathbf{Y}}{2}, L\right)\right)\Gamma d\mathbf{Y} = 0 \tag{4.31}$$

$$\implies 2ik\frac{\partial W}{\partial L} + 2i\mathbf{P}\cdot\nabla_{\mathbf{X}}W + k^2\left[\int e^{i\mathbf{P}\cdot\mathbf{Y}}\mu\left(\mathbf{X} - \frac{\mathbf{Y}}{2}, L\right)\Gamma\left(L, \mathbf{X}, \mathbf{Y}; \xi, \eta; k\right)d\mathbf{Y} - \int e^{i\mathbf{P}\cdot\mathbf{Y}}\mu\left(\mathbf{X} + \frac{\mathbf{Y}}{2}, L\right)\Gamma\left(L, \mathbf{X}, \mathbf{Y}; \xi, \eta; k\right)d\mathbf{Y}\right] = 0 \tag{4.32}$$

which after using the convolution theorem for the Fourier transform[4] becomes:

$$\implies 2ik\frac{\partial W}{\partial L} + 2i\mathbf{P}\cdot\nabla_{\mathbf{X}}W + k^2\int e^{-i\mathbf{Q}\cdot\mathbf{X}}\hat{\mu}\left(\mathbf{Q}, L\right)\left[W\left(L, \mathbf{X}, \mathbf{P} + \frac{\mathbf{Q}}{2}; \xi, \eta; k\right) - W\left(L, \mathbf{X}, \mathbf{P} - \frac{\mathbf{Q}}{2}; \xi, \eta; k\right)\right]d\mathbf{Q} = 0 \tag{4.33}$$

where $\hat{\mu}\left(\mathbf{Q}, L\right)$ is the Fourier transform of $\mu\left(\mathbf{x}, L\right)$ in the direction $\mathbf{x}$. We also have initial conditions from the Fourier transform of Equation 4.29:

$$W\left(0, \mathbf{X}, \mathbf{P}; \xi, \eta; k\right) = \frac{1}{(2\pi)^d}e^{-i\mathbf{P}\cdot(\xi-\eta)}\delta\left(\mathbf{X} - \frac{\xi+\eta}{2}\right). \tag{4.34}$$

This all looks very messy but now to bring it all together!

[3] I will give small amount of intuition as to why this is a sensible choice. As described in Paper [17], the Wigner transform was was first proposed in 1932 by Eugene Wigner, to account for quantum corrections to classical statistical mechanics. The similarity of the Parabolic Equation (see Equation 4.9) to the Schrödinger Equation means that the Wigner transform has applications for the study of energy propagation and time reversal phenomena in the high frequency limit.

[4] e.g. for the first integral we recall that: $f * g = \mathcal{F}^{-1}\{\mathcal{F}\{f\}\cdot\mathcal{F}\{g\}\}$ we then set $f = e^{i\mathbf{P}\cdot\mathbf{Y}}\Gamma\left(L, \mathbf{X}, \mathbf{Y}; \xi, \eta; k\right)$ and $g = \mu\left(\mathbf{X} - \frac{\mathbf{Y}}{2}, L\right)$ and work through the algebraic manipulations

Lemma 4.1.3. *We can recover* Γ *from* W *through Equation :*

$$\Gamma(L, \boldsymbol{y}, \boldsymbol{y}; \xi, \eta; k) = \int W(L, \boldsymbol{y}, \boldsymbol{P}, \xi, \eta; k) d\boldsymbol{P} \tag{4.35}$$

Proof. By definition:

$$\Gamma(L, \mathbf{X}, \mathbf{Y}; \xi, \eta; k) = \int e^{-i\mathbf{P}\cdot\mathbf{Y}} W(L, \mathbf{X}, \mathbf{P}, \xi, \eta; k) d\mathbf{P} \tag{4.36}$$

$$\implies \Gamma(L, \mathbf{x}, \mathbf{y}; \xi, \eta; k) = \int e^{-i\mathbf{P}\cdot(\frac{\mathbf{x}-\mathbf{y}}{2})} W(L, \frac{\mathbf{x}+\mathbf{y}}{2}, \mathbf{P}, \xi, \eta; k) d\mathbf{P} \tag{4.37}$$

$$\tag{4.38}$$

Setting $\mathbf{x} = \mathbf{y}$ completes the proof. □

Corollary 4.1.3.1. *We can thus define the back propagated field*

$$\psi^B(\xi, L; k) = \int\int \chi_A(\boldsymbol{y}) \overline{\psi_0(\eta, k)} \left(\int W(L, \boldsymbol{y}, \boldsymbol{P}, \xi, \eta; k) d\boldsymbol{P} \right) d\eta \; d\boldsymbol{y} \tag{4.39}$$

Proof. Follows by substituting Equation 4.35 into Equation 4.39. □

4.1.2.3 Homogeneous Medium

We bring this all back to reality and calculate the back-propagated wave for two special cases of a homogeneous medium ($\mu = 0$):

Lemma 4.1.4. *For a homogeneous medium and a source wave described by a delta function in space we have that:*

1. *For a finite aperture time reversal mirror (TRM) in one dimension,* $d = 1$ *and of size* a *centred at* $y = 0$*:*

$$\chi_A(y) = \begin{cases} 1, & \text{if } y \in [-\frac{a}{2}, \frac{a}{2}] \\ 0, & \text{else} \end{cases} \implies \psi^B(\xi, L; k) = \frac{1}{\pi\xi} \sin\left(\frac{k\xi a}{2L}\right) e^{\frac{ik\xi^2}{2L}}. \tag{4.40}$$

2. *If* χ_A *is a normalised isotropic Gaussian with variance* a *centred at* $\boldsymbol{y} = 0$ *but no assumptions on dimension, then we have :*

$$\chi_A(\boldsymbol{y}) \sim \frac{1}{(2\pi a^2)^{\frac{d}{2}}} e^{-\frac{|y|^2}{2a^2}} \implies \psi^B(\xi, L; k) = \left(\frac{k}{2\pi L}\right)^d e^{-\frac{a^2k^2|\xi|^2}{2L^2}} e^{\frac{ik|\xi|^2}{2L}}. \tag{4.41}$$

3. *In both cases we get a resolution proportional to* $\dfrac{\lambda L}{a}$.

Remark 10. We consider the case where the aperture function is a Gaussian because this will be easier to compare with the inhomogeneous case: the edges of a finite aperture will cause complications. It also allows us to more easily consider multiple dimensions.

Proof. For a homogeneous medium we can set $\mu = 0$ and thus the solution to Equation 4.33 with initial conditions given by Equation 4.34 can be found using the method of characteristics:

$$W(L, \mathbf{X}, \mathbf{P}, \xi, \eta; k) = \frac{1}{(2\pi)^d} e^{-i\mathbf{P}\cdot(\xi-\eta)} \delta\left(\mathbf{X} - \frac{L\mathbf{P}}{k} - \frac{\xi+\eta}{2}\right). \tag{4.42}$$

In order to check it does indeed satisfy the differential Equation one could either suspend belief and consider the derivative of the delta function of more rigorously consider W as a distribution and it follows very quickly.

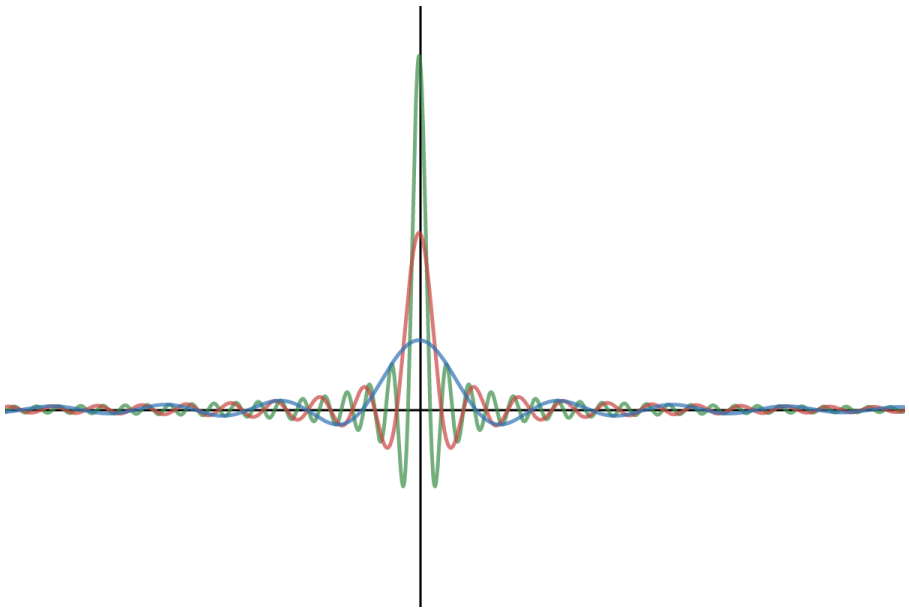

Figure 4.2: A plot of $\frac{\sin(x/a)}{x}$ for small values of a.

From Equation 4.35 we get that:

$$\Gamma(L,\mathbf{y},\mathbf{y};\xi,\eta;k) = \int \frac{1}{(2\pi)^d} e^{-i\mathbf{P}\cdot(\xi-\eta)} \delta\left(\mathbf{y} - \frac{L\mathbf{P}}{k} - \frac{\xi+\eta}{2}\right) d\mathbf{P} = \frac{1}{(2\pi)^d}\left(\frac{k}{L}\right)^d e^{-\frac{k}{L}\left(\mathbf{y}-\frac{\xi+\eta}{2}\right)\cdot(\xi-\eta)} \tag{4.43}$$

and thus

$$\psi^B(\xi,L;k) = \int\int \chi_A(\mathbf{y})\overline{\psi_0(\eta,k)}\left(\frac{1}{(2\pi)^d}\left(\frac{k}{L}\right)^d e^{-\frac{ik}{L}\left(\mathbf{y}-\frac{\xi+\eta}{2}\right)\cdot(\xi-\eta)}\right) d\eta\, d\mathbf{y} \tag{4.44}$$

$$\implies = \left(\frac{k}{L}\right)^d \int\left(\int \frac{1}{(2\pi)^d} e^{-\frac{ik}{L}(\mathbf{y})\cdot(\xi-\eta)}\chi_A(\mathbf{y})d\mathbf{y}\right) e^{\frac{ik}{L}\left(\frac{\xi+\eta}{2}\right)\cdot(\xi-\eta)}\overline{\psi_0(\eta,k)}d\eta \tag{4.45}$$

$$\implies = \left(\frac{k}{L}\right)^d \int \hat{\chi}_A\left(\frac{k}{L}(\eta-\xi)\right) e^{\frac{ik}{L}\left(\frac{\xi^2-\eta^2}{2}\right)}\overline{\psi_0(\eta,k)}d\eta. \tag{4.46}$$

where $\hat{\chi}$ is the Fourier transform of the function χ. Hence, if we consider that the source is a δ function in space i.e. that $\psi_0(\eta) = \delta(\eta)$ hence:

$$\psi^B(\xi,L;k) = \left(\frac{k}{L}\right)^d \int \hat{\chi}_A\left(\frac{k}{L}(\eta-\xi)\right) e^{\frac{ik}{L}\left(\frac{\xi^2-\eta^2}{2}\right)}\delta(\eta)d\eta \tag{4.47}$$

$$\implies = \left(\frac{k}{L}\right)^d \hat{\chi}_A\left(\frac{-\xi k}{L}\right) e^{\frac{ik\xi^2}{2L}}. \tag{4.48}$$

Finite TRM

$$\chi_A(y) = \begin{cases} 1, & \text{if } y \in [-\frac{a}{2},\frac{a}{2}] \\ 0, & \text{else} \end{cases} \implies \hat{\chi}_A(P) = \frac{1}{2\pi}\int_{-\frac{a}{2}}^{\frac{a}{2}} e^{iPy}dy = \frac{1}{\pi\xi}\sin\left(\frac{Pa}{2}\right). \tag{4.49}$$

Hence,

$$\psi^B(\xi,L;k) = \frac{1}{\pi\xi}\sin\left(\frac{k\xi a}{2L}\right) e^{\frac{ik\xi^2}{2L}} \tag{4.50}$$

We recall from our assumptions that $\lambda \propto \frac{1}{k} \ll a \ll L \implies \frac{ka}{L}$ is large. Hence, consider the functions plotted in Figure 4.2 we see that due to the decay away from the origin a suitable measure

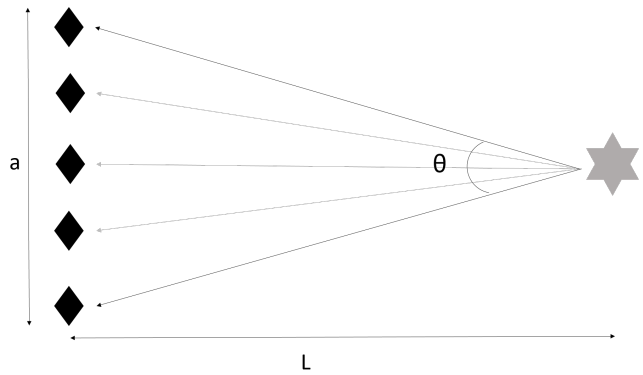

Figure 4.3: Diagram to help justify the resolution of the back propagated wave in the case of a finite aperture array and when the source is a δ function in space

of resolution is the difference between the origin and the first zero of the phase conjugated back propagated field:

$$\xi_F = \frac{2\pi L}{ka} = \frac{\lambda L}{a}. \tag{4.51}$$

Gaussian TRM Let:

$$\chi_A(\mathbf{y}) \sim \frac{1}{(2\pi a^2)^{\frac{d}{2}}} e^{-\frac{|y|^2}{2a^2}} \tag{4.52}$$

$$\implies \hat{\chi}_A(\mathbf{P}) = \left(\frac{1}{2\pi}\right)^d e^{-\frac{a^2\mathbf{P}^2}{2}} \tag{4.53}$$

Thus we can compute the back propagated wave:

$$\psi^B(\xi, L; k) = \left(\frac{k}{L}\right)^d \hat{\chi}_A\left(\frac{-\xi k}{L}\right) e^{\frac{ik|\xi|^2}{2L}} \tag{4.54}$$

$$= \left(\frac{k}{2\pi L}\right)^d e^{-\frac{a^2k^2|\xi|^2}{2L^2}} e^{\frac{ik|\xi|^2}{2L}} \tag{4.55}$$

Which is another Gaussian and has a resolution proportional to the variance of the Gaussian, i.e. proportional to $\frac{L}{a} \propto \frac{\lambda L}{a}$ as in the finite aperture case.

□

Remark 11. A few comments on the resolution $\frac{\lambda L}{a}$:

- Increasing the size of the aperture a will increase the amount of information on the forward propagating wave and thus improving the resolution of the reconstruction
- Increasing L will reduce the proportion of waves propagated from the point source that reach the array, reducing information available and thus worsening the resolution.
- With the help of hindsight we can also justify the linear relationship by considering Figure 4.3. We can say:

  $$\theta \approx \tan(\theta) = \frac{a}{2L}. \tag{4.56}$$

  Where θ is small because $a \ll L$. Hence, we consider the "amount of information" received by the array to be proportional to be the range of angles, for which if a wave is propagated from the source with that angle it will hit the array. This amount of information is given by Equation 4.56 and is thus proportional to $\frac{a}{L}$. We then take the amount of information to be inversely proportional to the error and we have a hand wavy explanation for the result.

4.1.2.4 Inhomogeneous media

We expand on the assumptions given at the beginning of this chapter and introduce scaling parameters in order to more easily study the effects of random inhomogeneities:

- The wavelength $\lambda \ll L$, the propagation distance and define the dimensionless variable $\epsilon = \frac{\lambda}{L} \ll 1$.
- The wavelength $\lambda \lesssim l$, the correlation length.
- The fluctuations $\mu = n^2 - 1$ are weak and isotropic i.e. $|\mu| \approx \sqrt{\epsilon}$.

We want to analyse the long-distance and long-time propagation and so rescale $\mathbf{x} \to \frac{\mathbf{x}}{\epsilon}$ and $L \to \frac{L}{\epsilon}$. We can thus rescale the functions that we have defined previously:

- $G^\epsilon(L_0, \mathbf{x}; \xi; k) = G(\frac{L_0}{\epsilon}, \frac{\mathbf{x}}{\epsilon}; \xi; k)$
- $\Gamma^\epsilon(L, \mathbf{x}, \mathbf{y}; \xi, \eta; k) = G^\epsilon(L, 0; \mathbf{x}, \xi; k)\overline{G^\epsilon(L, 0; \mathbf{y}, \eta; k)}$
- Where Γ^ϵ satisfies

$$2ik\epsilon\frac{\partial\Gamma^\epsilon}{\partial L} + \epsilon^2(\Delta_{\mathbf{x}} - \Delta_{\mathbf{y}})\Gamma^\epsilon + k^2\sqrt{\epsilon}\left(\mu\left(\frac{\mathbf{x}}{\epsilon}, \frac{L}{\epsilon}\right) - \mu\left(\frac{\mathbf{y}}{\epsilon}, L\right)\right)\Gamma^\epsilon = 0 \tag{4.57}$$

  with initial conditions

$$\Gamma^\epsilon(0, \mathbf{x}, \mathbf{y}; \xi, \eta; k) = \frac{1}{\epsilon}\delta\left(\frac{\mathbf{x} - \xi}{\epsilon}\right)\delta\left(\frac{\mathbf{y} - \eta}{\epsilon}\right). \tag{4.58}$$

Again, as in Section 4.1.2.2, we make a change of variables, but this time we have to think carefully about where to place the factors of ϵ. In general we are interested in $\Gamma^\epsilon(L, \mathbf{y}, \mathbf{y}; \xi, \eta; k)$ within a few wavelengths of the point $\mathbf{y}$. We can place a magnifying glass on this neighbourhood by letting:

$$\left.\begin{array}{c}\mathbf{X} = \frac{\mathbf{x}+\mathbf{y}}{2} \\ \epsilon\mathbf{Y} = \mathbf{y} - \mathbf{x}\end{array}\right\} \iff \left\{\begin{array}{l}\mathbf{x} = \mathbf{X} - \frac{\epsilon\mathbf{Y}}{2} \\ \mathbf{y} = \mathbf{X} + \frac{\epsilon\mathbf{Y}}{2}\end{array}\right. \tag{4.59}$$

Which allows us to simplify $\nabla_{\mathbf{x}} - \nabla_{\mathbf{y}} = (\nabla_{\mathbf{x}} - \nabla_{\mathbf{y}})(\nabla_{\mathbf{x}} - \nabla_{\mathbf{y}}) = -\frac{2}{\epsilon}\nabla_{\mathbf{X}}\nabla_{\mathbf{Y}}$. As before define $W^\epsilon(L, \mathbf{X}, \mathbf{P}; \xi, \eta; k)$ to be the Fourier transform with respect to $\mathbf{Y}$ of $\Gamma^\epsilon(L, \mathbf{X}, \mathbf{Y}; \xi, \eta; k)$. We get that:

- Differential Equation for Γ^ϵ:

$$2ik\frac{\partial\Gamma^\epsilon}{\partial L} - 2\nabla_{\mathbf{X}}\nabla_{\mathbf{Y}}\Gamma^\epsilon + \frac{k^2}{\sqrt{\epsilon}}\left(\mu\left(\frac{\mathbf{X}}{\epsilon} - \frac{\mathbf{Y}}{2}, \frac{L}{\epsilon}\right) - \mu\left(\frac{\mathbf{X}}{\epsilon} + \frac{\mathbf{Y}}{2}, L\right)\right)\Gamma^\epsilon = 0. \tag{4.60}$$

- Initial conditions for Γ^ϵ:

$$\Gamma^\epsilon(0, \mathbf{X}, \mathbf{Y}; \xi, \eta; k) = \frac{1}{\epsilon}\delta\left(\frac{\mathbf{X} - \xi}{\epsilon} - \frac{\mathbf{Y}}{2}\right)\delta\left(\frac{\mathbf{X} - \eta}{\epsilon} + \frac{\mathbf{Y}}{2}\right). \tag{4.61}$$

- Differential equation for W^ϵ:

$$\begin{aligned}&k\frac{\partial W^\epsilon}{\partial L} + \mathbf{P}\cdot\nabla_{\mathbf{X}}W^\epsilon \\ &= \frac{ik^2}{2\sqrt{\epsilon}}\int e^{-i\mathbf{Q}\cdot\frac{\mathbf{X}}{\epsilon}}\hat{\mu}\left(\mathbf{Q}, \frac{L}{\epsilon}\right)\left[W^\epsilon(L, \mathbf{X}, \mathbf{P} + \frac{\mathbf{Q}}{2}; \xi, \eta; k) - W^\epsilon(L, \mathbf{X}, \mathbf{P} - \frac{\mathbf{Q}}{2}; \xi, \eta; k)\right]d\mathbf{Q}.\end{aligned} \tag{4.62}$$

- Initial conditions for W^ϵ:

$$W^\epsilon(0, \mathbf{X}, \mathbf{P}; \xi, \eta; k) = \frac{1}{(2\pi)^d}e^{-i\mathbf{P}\cdot\frac{\xi-\eta}{\epsilon}}\delta\left(\mathbf{X} - \frac{\xi + \eta}{2}\right). \tag{4.63}$$

So what has been the point of formulating things with the Wigner transform? With random media we get random results and therefore we will be investigating statistics such as the mean and variance of the back propagated wave. The Wigner transform has an important property described in the following lemma:

Lemma 4.1.5. *We claim that for W^ϵ, defined above:*

$$\langle W^\epsilon(L, \boldsymbol{X}, \boldsymbol{P}; \xi, \eta; k)\rangle \to W(L, \boldsymbol{X}, \boldsymbol{P}; \xi, \eta; k) \text{ as } \epsilon \to 0 \tag{4.64}$$

Where W satisfies the Equation:

$$k\frac{\partial W}{\partial L} + \boldsymbol{P}\cdot\nabla_{\boldsymbol{X}} W = \frac{\pi k^3}{4}\int \hat{R}\left(\frac{\boldsymbol{P}^2 - \boldsymbol{Q}^2}{2k}, \boldsymbol{P} - \boldsymbol{Q}\right)\left[W(L, \boldsymbol{X}, \boldsymbol{Q}; \xi, \eta; k) - W(L, \boldsymbol{X}, \boldsymbol{P}; \xi, \eta; k)\right] d\boldsymbol{Q}. \tag{4.65}$$

With initial conditions

$$W(0, \boldsymbol{X}, \boldsymbol{P}; \xi, \eta; k) = \frac{1}{(2\pi)^d} e^{-i\boldsymbol{P}\cdot\frac{\xi-\eta}{\epsilon}}\delta\left(\boldsymbol{X} - \frac{\xi+\eta}{2}\right). \tag{4.66}$$

Where $R(z, \boldsymbol{x}) = \langle\mu(\eta, \boldsymbol{y})\mu(\eta + z, \boldsymbol{y} + \boldsymbol{x})\rangle$ and $\hat{R}(p, \boldsymbol{P})$ is its Fourier transform with respect to $(z, \boldsymbol{x})$.

Remark 12. We note the remaining ϵ dependence in the initial conditions despite having taken the limit as $\epsilon \to 0$. This seems odd, but at the moment it is not clear how to best take the limit and we still want to emphasise the diffraction effects, which are important for time-reversal.

Proof. Consider now Paper [3] and Paper [17] and we expand on their explanation. We have defined W^ϵ to be

$$W^\epsilon(L, \mathbf{X}, \mathbf{P}, \xi, \eta; k) = \frac{1}{(2\pi)^d}\int e^{i\mathbf{P}\cdot\mathbf{Y}}\Gamma^\epsilon(L, \mathbf{X}, \mathbf{Y}; \xi, \eta; k)d\mathbf{Y} \tag{4.67}$$

$$= \frac{1}{(2\pi)^d}\int e^{i\mathbf{P}\cdot\mathbf{Y}} G^\epsilon(L, 0; \mathbf{x}, \xi; k)\overline{G^\epsilon(L, 0; \mathbf{y}, \eta; k)}d\mathbf{Y} \tag{4.68}$$

$$= \frac{1}{(2\pi)^d}\int e^{i\mathbf{P}\cdot\mathbf{Y}} G\left(\frac{L_0}{\epsilon}, \frac{\mathbf{x}}{\epsilon}; \xi; k\right)\overline{G\left(\frac{L_0}{\epsilon}, \frac{\mathbf{y}}{\epsilon}; \eta; k\right)}d\mathbf{Y} \tag{4.69}$$

The family of functions W^ϵ is bounded in the space of Schwartz distributions $S'(\mathbb{R}^d, \mathbb{R}^d)$ if the functions G^ϵ or uniformly bounded in $L^2(\mathbb{R}^d)$

Therefore there exists a subsequence ϵ_k such that W^{ϵ_k} converges weakly as $k \to \infty$ to a limit W.

The differential equation (Equation 4.65) is non-obvious to derive but doing so does not add much understanding so the proof is omitted. For more in depth discussion see Paper [17].

We leave the initial conditions unchanged: see Remark 12.

□

We now restrict our attention to the behaviour of the time reversed field in the vicinity of the source. We do this assume that the frequencies $\eta - \xi = O(\epsilon)$. Thus we can ignore the ϵ in the initial conditions giving:

$$W(0, \mathbf{X}, \mathbf{P}; \xi, \eta; k) = \frac{1}{(2\pi)^d} e^{-i\mathbf{P}\cdot(\xi-\eta)}\delta\left(\mathbf{X} - \frac{\xi+\eta}{2}\right). \tag{4.70}$$

4.1.2.5 Beam Approximation

We now consider in more detail the correlation function $R(z, \mathbf{x}) = \langle\mu(\eta, \mathbf{y})\mu(\eta + z, \mathbf{y} + \mathbf{x})\rangle$. We have assumed that the size of our TRM is small ($a \ll L$) and thus only waves that remain near the z-axis will contribute significantly to the back-propagated field, all other waves will not reach the array. This makes sure that the power spectral density, $\hat{R}(p, \mathbf{P})$, is peaked near zero, in the transverse direction.

Lemma 4.1.6. *If the power spectral density, $\hat{R}(p, \boldsymbol{P})$, is peaked near zero, in the transverse direction we can approximate W to be the solution to*

$$k\frac{\partial W}{\partial L} + \boldsymbol{P}\cdot\nabla_{\boldsymbol{X}} W = \gamma k^3 \nabla^2_{\boldsymbol{P}} W(\boldsymbol{P}) \tag{4.71}$$

$$W(0, \boldsymbol{X}, \boldsymbol{P}; \xi, \eta; k) = \frac{1}{(2\pi)^d} e^{-i\boldsymbol{P}\cdot(\xi-\eta)} \delta\left(\boldsymbol{X} - \frac{\xi+\eta}{2}\right) \tag{4.72}$$

where γ is a constant.

Proof. $\hat{R}(p, \mathbf{P})$ peaked near zero means that in the integral in Equation 4.65 we consider $\hat{R}(\frac{\mathbf{P}^2-\mathbf{Q}^2}{2k}, \mathbf{P}-\mathbf{Q}) \approx 0$ for $P \neq Q$. Thus we can expand $W(L, \mathbf{X}, \mathbf{Q}; \xi, \eta; k) = W(L, \mathbf{X}, \mathbf{P} + (\mathbf{Q}-\mathbf{P}); \xi, \eta; k)$ where $(\mathbf{Q}-\mathbf{P})$ is small. We thus rewrite Equation 4.65 to get:

$$\begin{aligned} k\frac{\partial W}{\partial L} + \mathbf{P}\cdot\nabla_{\mathbf{X}} W = \frac{\pi k^3}{4}\int \hat{R}\left(\frac{\mathbf{P}^2-\mathbf{Q}^2}{2k}, \mathbf{P}-\mathbf{Q}\right) \\ \times\left[\nabla_{\mathbf{P}} W(L, \mathbf{X}, \mathbf{P}; \xi, \eta; k)\cdot(\mathbf{Q}-\mathbf{P}) + \frac{1}{2}\nabla_{\mathbf{P}}\nabla_{\mathbf{P}} W(L, \mathbf{X}, \mathbf{P}; \xi, \eta; k)\cdot(\mathbf{Q}-\mathbf{P})^2\right] d\mathbf{Q} \end{aligned} \tag{4.73}$$

we note that $\hat{R}$ is even and so the first term in the integral integrates out to zero and we are left with the second order term:

$$k\frac{\partial W}{\partial L} + \mathbf{P}\cdot\nabla_{\mathbf{X}} W = \frac{\pi k^3}{8}\nabla^2_{\mathbf{P}} W(L, \mathbf{X}, \mathbf{P}; \xi, \eta; k)\int \hat{R}\left(\frac{\mathbf{P}^2-\mathbf{Q}^2}{2k}, \mathbf{P}-\mathbf{Q}\right)|\mathbf{P}-\mathbf{Q}|^2 d\mathbf{Q} \tag{4.74}$$

$$\implies k\frac{\partial W}{\partial L} + \mathbf{P}\cdot\nabla_{\mathbf{X}} W = \frac{\pi k^3}{8} D(\mathbf{P})\nabla^2_{\mathbf{P}} W(\mathbf{P}) \tag{4.75}$$

Where we define the function:

$$D(\mathbf{P}) = \int \hat{R}\left(\frac{\mathbf{P}^2-\mathbf{Q}^2}{2k}, \mathbf{P}-\mathbf{Q}\right)|\mathbf{P}-\mathbf{Q}|^2 d\mathbf{Q}. \tag{4.76}$$

In many interesting scaling limits this turns out to be constant so we call it the wave number diffusion constant, D. Additionally, define constant $\gamma = \frac{\pi D}{8}$. This simplifies our equations, so along with the initial conditions in Equation 4.70, we get:

$$k\frac{\partial W}{\partial L} + \mathbf{P}\cdot\nabla_{\mathbf{X}} W = \gamma k^3 \nabla^2_{\mathbf{P}} W(\mathbf{P}) \tag{4.77}$$

$$W(0, \mathbf{X}, \mathbf{P}; \xi, \eta; k) = \frac{1}{(2\pi)^d} e^{-i\mathbf{P}\cdot(\xi-\eta)} \delta\left(\mathbf{X} - \frac{\xi+\eta}{2}\right) \tag{4.78}$$

□

Lemma 4.1.7. *Equations 4.71 and 4.72 have solution:*

$$\begin{aligned} W(L, \boldsymbol{X}, \boldsymbol{P}; \xi, \eta; k) = \left(\frac{k}{L(2\pi)^2}\right)^d \int e^{-i(\frac{k(\boldsymbol{u}+(\xi-\eta))}{L})\cdot(\frac{\xi+\eta}{2})} \\ e^{-\gamma k^2\left(\frac{1}{3}|\frac{\boldsymbol{u}+(\xi-\eta)}{L}|^2 L^3 - L^2\left((\frac{\boldsymbol{u}+(\xi-\eta)}{L})\cdot\boldsymbol{u}\right)+|\boldsymbol{u}|^2 L\right)} e^{i(\frac{k(\boldsymbol{u}+(\xi-\eta))}{L})\cdot\boldsymbol{X}} e^{i\boldsymbol{u}\cdot\boldsymbol{P}} d\boldsymbol{u}. \end{aligned} \tag{4.79}$$

Proof. First we take the Fourier Transform of Equations 4.71 and 4.72 with respect to variables $\mathbf{X}$ and $\mathbf{P}$ with respective Fourier variables $\mathbf{u}$ and $\mathbf{v}$

$$\frac{\partial \hat{W}}{\partial L} + \frac{\mathbf{v}}{k}\cdot\nabla_{\mathbf{u}}\hat{W} = -\gamma k^2|\mathbf{u}|^2\hat{W} \tag{4.80}$$

$$\hat{W}(0, \mathbf{u}, \mathbf{v}; \xi, \eta; k) = e^{-i\mathbf{v}\cdot(\frac{\xi+\eta}{2})}\delta\left(\mathbf{u} + (\xi-\eta)\right) \tag{4.81}$$

We can now solve this using the method of characteristics to get:

$$\hat{W}(L,\mathbf{u},\mathbf{v};\xi,\eta;k) = e^{-i\mathbf{v}\cdot(\frac{\xi+\eta}{2})}\delta\left(-\frac{L\mathbf{v}}{k}+\mathbf{u}+(\xi-\eta)\right)e^{-\gamma k^2\left(\frac{|\mathbf{v}|^2L^3}{3k^2}+L^2\left(-\frac{\mathbf{v}\cdot\mathbf{u}}{k}\right)+|\mathbf{u}|^2L\right)} \tag{4.82}$$

We now need to Fourier Transform this back:

$$W(L,\mathbf{X},\mathbf{P};\xi,\eta;k) = \frac{1}{(2\pi)^{2d}}\int\int e^{-i\mathbf{v}\cdot(\frac{\xi+\eta}{2})}\delta\left(-\frac{L\mathbf{v}}{k}+\mathbf{u}+(\xi-\eta)\right) e^{-\gamma k^2\left(\frac{|\mathbf{v}|^2L^3}{3k^2}+L^2\left(-\frac{\mathbf{v}\cdot\mathbf{u}}{k}\right)+|\mathbf{u}|^2L\right)}e^{i\mathbf{v}\cdot\mathbf{X}}e^{i\mathbf{u}\cdot\mathbf{P}}d\mathbf{u}d\mathbf{v}. \tag{4.83}$$

Evaluating the $d\mathbf{v}$ integral, we get:

$$W(L,\mathbf{X},\mathbf{P};\xi,\eta;k) = \frac{1}{(2\pi)^{2d}}\left(\frac{k}{L}\right)^d\int e^{-i(\frac{k(\mathbf{u}+(\xi-\eta))}{L})\cdot(\frac{\xi+\eta}{2})} e^{-\gamma k^2\left(\frac{|(\frac{k(\mathbf{u}+(\xi-\eta))}{L})|^2L^3}{3k^2}+L^2\left(-\frac{(\frac{k(\mathbf{u}+(\xi-\eta))}{L})\cdot\mathbf{u}}{k}\right)+|\mathbf{u}|^2L\right)}e^{i(\frac{k(\mathbf{u}+(\xi-\eta))}{L})\cdot\mathbf{X}}e^{i\mathbf{u}\cdot\mathbf{P}}d\mathbf{u}. \tag{4.84}$$

Which when neatened up gives the solution required.

□

We can then finally get solutions for the averaged back-propagated wave and an effective amplitude:

Lemma 4.1.8. *Under the above assumptions we get that:*

- *For a Gaussian TRM*

$$\langle\psi^B(\xi,L;k)\rangle = \left(\frac{k}{2\pi L}\right)^d e^{-\gamma Lk^2|\xi|^2}e^{-\frac{a^2k^2|\xi|^2}{2L^2}}e^{\frac{ik|\xi|^2}{2L}} \tag{4.85}$$

  and thus

$$a_e = a\sqrt{1+\frac{2\gamma L^3}{a^2}} > a \tag{4.86}$$

- *For a finite TRM*

$$\langle\psi^B(\xi,L;k)\rangle = \frac{1}{\pi\xi}\sin\left(\frac{k\xi a}{2L}\right)e^{\frac{ik\xi^2}{2L}}e^{-\gamma Lk^2\xi^2} \tag{4.87}$$

  and thus $a_e > a$

Remark 13. The **effective aperture** a_e is the value such that the time-reversed and back-propagated field can be calculated exactly as in the homogeneous case by replacing a with a_e.

Proof. Using the Fourier and Inverse Fourier Transform we can state that for well behaved functions f:

$$f(\mathbf{y}) = \frac{1}{(2\pi)^d}\int\int f(\mathbf{x})e^{-i\mathbf{k}\cdot\mathbf{x}}d\mathbf{x}e^{i\mathbf{k}\cdot\mathbf{y}}d\mathbf{k} \tag{4.88}$$

$$\implies (2\pi)^d f(\mathbf{0}) = \int\int f(\mathbf{x})e^{-i\mathbf{k}\mathbf{x}}d\mathbf{x}d\mathbf{k} \tag{4.89}$$

Using this identity, Equation 4.35 and the solution for W given by Equation 4.79 we get that:

$$\Gamma(L,\mathbf{y},\mathbf{y};\xi,\eta;k) = \int W(L,\mathbf{y},\mathbf{P},\xi,\eta;k)d\mathbf{P} \tag{4.90}$$

$$= \left(\frac{k}{2\pi L}\right)^d e^{-i\frac{k}{L}(\mathbf{y}-\frac{\xi+\eta}{2})\cdot(\xi-\eta)}e^{-\gamma k^2L(\xi-\eta)^2}. \tag{4.91}$$

where we have pulled the extra factor of 3 into the constant γ. Then using equation 4.39 we get that:

$$\langle \psi^B(\xi, L; k) \rangle = \int\int \chi_A(\mathbf{y}) \overline{\psi_0(\eta, k)} \int W(L, \mathbf{y}, \mathbf{P}, \xi, \eta; k) d\mathbf{P} d\eta \; d\mathbf{y} \tag{4.92}$$

$$= \int\int \chi_A(\mathbf{y}) \overline{\psi_0(\eta, k)} \left(\frac{k}{2\pi L}\right)^d e^{-i\frac{k}{L}(\mathbf{y} - \frac{\xi+\eta}{2})\cdot(\xi-\eta)} e^{-\gamma k^2 L(\xi-\eta)^2} d\eta \; d\mathbf{y} \tag{4.93}$$

$$= \left(\frac{k}{L}\right)^d e^{\frac{ik\xi^2}{2L}} \int \left[\int \left(\frac{1}{2\pi}\right)^d \chi_A(\mathbf{y}) e^{-i\frac{k}{L}\mathbf{y}\cdot(\xi-\eta)} d\mathbf{y} \right] e^{\frac{-ik\eta^2}{2L}} \overline{\psi_0(\eta, k)} e^{-\gamma L k^2 (\xi-\eta)^2} d\eta \tag{4.94}$$

$$= \left(\frac{k}{L}\right)^d e^{\frac{ik\xi^2}{2L}} \int \hat{\chi}_A(\frac{k}{L}(\eta - \xi)) e^{-\frac{ik\eta^2}{2L}} \overline{\psi_0(\eta, k)} e^{-\gamma L k^2 (\xi-\eta)^2} d\eta \tag{4.95}$$

We compare this to results earlier, and Equation 4.46 in particular to note that the effect of the random medium is the Gaussian factor $e^{-\gamma L k^2 (\xi-\eta)^2}$.

Gaussian TRM Consider a point source and a Gaussian aperture defined in Equation 4.53:

$$\chi_A(\mathbf{y}) \sim \frac{1}{(2\pi a^2)^{\frac{d}{2}}} e^{-\frac{|y|^2}{2a^2}} \tag{4.96}$$

$$\implies \hat{\chi}_A(\mathbf{P}) = \left(\frac{1}{2\pi}\right)^d e^{-\frac{a^2\mathbf{P}^2}{2}}. \tag{4.97}$$

Hence, subbing this into Equation 4.5

$$\langle \psi^B(\xi, L; k) \rangle = \left(\frac{k}{2\pi L}\right)^d e^{\frac{ik\xi^2}{2L}} \int e^{-\frac{a^2(k(\eta-\xi))^2}{2L^2}} e^{\frac{ik\eta^2}{2L}} \delta(\eta) e^{-\gamma L k^2 (\xi-\eta)^2} d\eta \tag{4.98}$$

$$= \left(\frac{k}{2\pi L}\right)^d e^{-\gamma L k^2 |\xi|^2} e^{-\frac{a^2 k^2 |\xi|^2}{2L^2}} e^{\frac{ik|\xi|^2}{2L}} \tag{4.99}$$

Which we can compare to what we got in the homogeneous case, specifically Equation 4.41, we can find the effective aperture for the mean-time harmonic wave:

$$a_e = a\sqrt{1 + \frac{2\gamma L^3}{a^2}} > a \tag{4.100}$$

Finite Aperture TRM Returning to Equation 4.49 we sub this into Equation 4.95 to get:

$$\langle \psi^B(\xi, L; k) \rangle = \frac{1}{\pi\xi} \sin\left(\frac{k\xi a}{2L}\right) e^{\frac{ik\xi^2}{2L}} e^{-\gamma L k^2 \xi^2}. \tag{4.101}$$

We note that both L and k are large and hence $e^{-\gamma L k^2 \xi^2}$ drops of quickly away from the origin, see Figure 4.4. The outermost curve is the case when $\frac{\sin(x)}{x} e^{-x^2}$ and the resolution is almost identically the one for homogeneous media. Larger values in the exponential give a smaller width of the peak and thus a higher resolution. A higher resolution than we have in the homogeneous case means that $a_e > a$, as required. □

Remark 14. The effective aperture cannot be increased to any arbitrary value. In order for our approximations to hold, especially the Beam approximation we require that $a_e \ll L$.

4.2 Statistical Stability

4.2.1 Qualitative description

[6] I realise that some of the waves shown are sometimes not uni-valued in time - this is not deliberate, it is just hard to draw random waves in powerpoint!

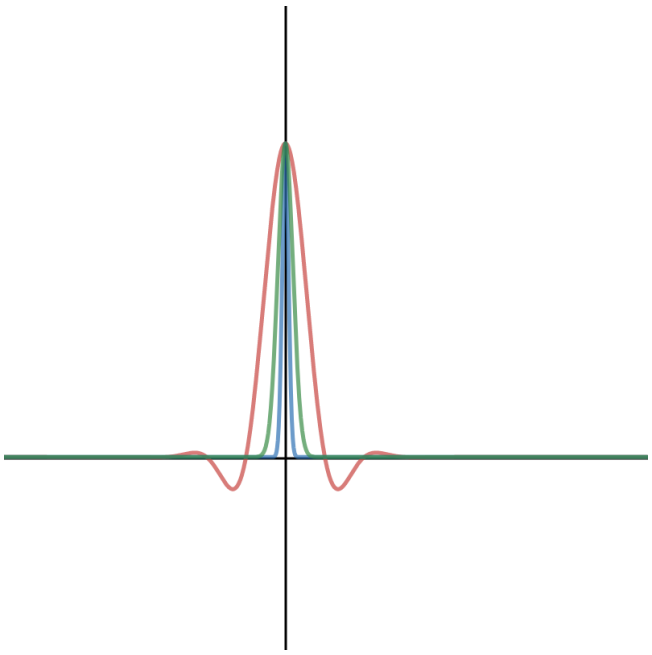

Figure 4.4: A plot of $\frac{\sin(x)}{x}e^{-Cx^2}$ for increasing values of C, the red line the smallest value, the blue line the highest.

Paper [13] describes the experiment shown in Figure 4.5. Identical thin steel rods are placed upright randomly in water to create a random media and the usual time-reversal experiment is set up with a source and an array of transducers. Time reversed wave traces the path of the forward waves back to the source, and as predicted above the experimenters saw a higher resolution with the random media than the homogeneous media.

What really surprised them however was the consistency in which they saw these results. Consider a pinball machine or a game of snooker: games with obstacles impeding the balls. Small deviations in initial trajectory will lead to significant differences in the end result, especially if multiple collisions are involved. We would expect a similar pattern for the waves in the experiment: small errors caused by the recording and re-emitting process would lead to significant variations in the trajectory of the time-reversed wave and a failure to refocus. However, even though the recorded signals where digitised and quantisation errors were introduced the focusing process still worked consistently.

Paper [13] explains this phenomena by recalling that waves propagate in all directions, following all possible trajectories. The final wave amplitude results from the interference (the sum of the amplitudes) of all possible trajectories and small errors only add linearly. The self-averaging properties of the back propagated wave means that the time-reversed wave consistently refocuses near the scatterer, despite the random media. A ball follows a well defined trajectory and even the smallest error could lead to the particle hitting an obstacle it was not meant to and changing the whole trajectory giving large, non linear, errors.

4.2.2 Quantitative Analysis

The qualitative explanation is more than a little hand wavy and we are interested where statistical stability comes up in the equations.

Paper [17] discusses statistical stability. It describes three potential asymptotic regimes, which relate to different assumptions in experimental configurations, that can be chosen and combined. We write them using our notation:

- High frequency limit: $\theta = \frac{L}{\lambda a^2} \to 0$
- White noise limit: $\epsilon = \frac{l}{L} \to 0$
- Broad beam limit $\delta = \frac{l}{a} \to 0$

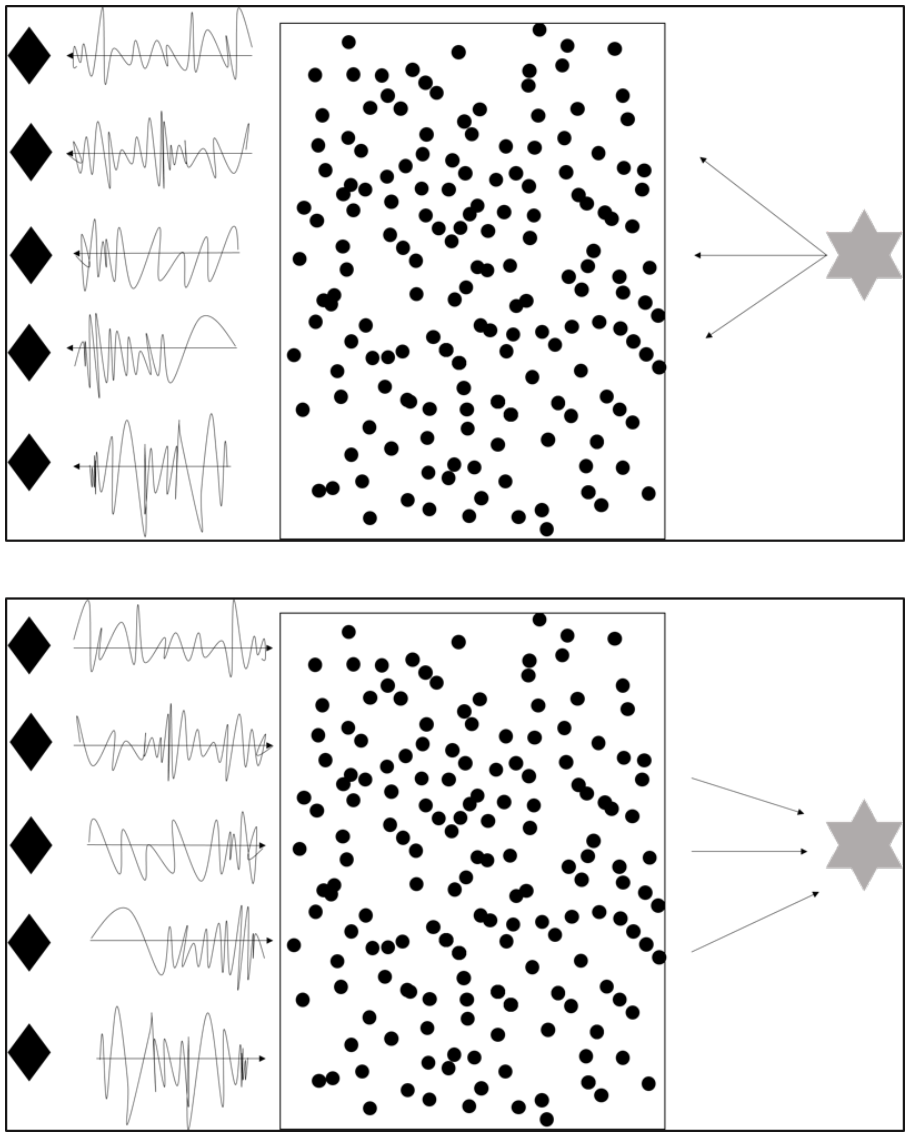

Figure 4.5: Time-reversal through around media generated by randomly distributed parallel steel rods in a water tank[6]. Describing experiment in Paper [13]

.

The assumptions given at the beginning of this chapter, that $\lambda \lessapprox l \ll a \ll L$, are equivalent to first taking the high frequency limit, then the white noise limit and then the broad beam limit. The paper shows in detail the derivation of statistical stability in these assumptions, however, this is a topic for a whole other essay. We instead follow Paper [4] to get a small flavour of the analysis:

Lemma 4.2.1. *For our assumptions we have that the wave is statistically stable in the space and time domain i.e. that:*

$$\Psi^B(L,\eta,k) \approx \langle \Psi^B(L,\eta,k)\rangle. \tag{4.102}$$

where

$$\Psi^B(L,\eta,k) = \int e^{i\omega t}\psi^B\left(L,\eta,\frac{\omega}{c_0}\right)d\omega. \tag{4.103}$$

Proof. We first note that for our assumptions: high frequencies, short correlation length (λ) and long propagation distance (L), we have the independence of the wave functions for different frequencies, i.e. for $k \neq k'$:

$$\langle \psi^B(L,\eta,k)\psi^B(L,\eta,k')\rangle \approx \langle \psi^B(L,\eta,k)\rangle\langle \psi^B(L,\eta,k')\rangle. \tag{4.104}$$

Thus

$$\langle (\Psi^B(L,\eta,k))^2\rangle = \langle \left(\int e^{i\omega t}\psi^B\left(L,\eta,\frac{\omega}{c_0}\right)d\omega\right)^2\rangle \tag{4.105}$$

$$= \int\int e^{i(\omega_1+\omega_2)t}\langle \psi^B\left(L,\eta,\frac{\omega_1}{c_0}\right)\psi^B\left(L,\eta,\frac{\omega_2}{c_0}\right)\rangle d\omega_1 d\omega_2 \tag{4.106}$$

$$\approx \int\int e^{i(\omega_1+\omega_2)t}\langle \psi^B\left(L,\eta,\frac{\omega_1}{c_0}\right)\rangle\langle \psi^B\left(L,\eta,\frac{\omega_2}{c_0}\right)\rangle d\omega_1 d\omega_2 \tag{4.107}$$

$$= \langle \Psi^B(L,\eta,k)\rangle^2 \tag{4.108}$$

we can now use Chebychev's inequality: for X (integrable) be a random variable with finite expected value μ and finite non-zero variance σ^2. Then for any real number $k \geq 0$:

$$\Pr(|X-\mu| \geq k\sigma) \leq \frac{1}{k^2}. \tag{4.109}$$

In our case we calculate the variance: $\sigma^2 = \langle \left(\Psi^B(L,\eta,k) - \langle \Psi^B(L,\eta,k)\rangle\right)^2\rangle = \langle (\Psi^B(L,\eta,k))^2\rangle - \langle \Psi^B(L,\eta,k)\rangle$. So that for any $\delta > 0$:

$$\Pr(|\Psi^B(L,\eta,k) - \langle \Psi^B(L,\eta,k)\rangle| \geq \delta) \leq \frac{\langle (\Psi^B(L,\eta,k))^2\rangle - \langle \Psi^B(L,\eta,k)\rangle}{\delta^2} \approx 0 \tag{4.110}$$

and hence we get the firework moment:

$$\Psi^B(L,\eta,k) \approx \langle \Psi^B(L,\eta,k)\rangle. \tag{4.111}$$

It is self averaging! □

As discussed in Paper [6], we have shown that with these assumptions we get significant multipathing and averaging over frequencies ω is like averaging over realisations of the random media making time reversal focusing statistically stable.

These are not the only assumptions we could have taken and indeed Paper [17] describes other asymptotic regimes that have been proven to give statistical stability including: taking first the white noise limit, then the high frequency limit and then the broad beam limit. There are cases where statistical stability is not realised and I think this is a good example of how the mathematical analysis can give a deeper understanding to the experimental observations.

4.3 Imaging in Random Media

In this Section we briefly consider the case of multiple scatterers in the media and follow Paper [6] to look at locating small scatters in a randomly inhomogeneous environment. As described in the DORT method, see Section 3.2.1, we are already able to experimentally back propagate the waves to focus on the scatterers but we are in general unable to do this numerically because we don't know the background Green's function. In order to image the area we need to develop such methods further, which is now possible as we can draw on what we have learnt about the statistical stability of back-propagated waves.

We start with an overview of relevant parts of Section 3 before looking at the case of random inhomogeneities.

As in Section 3.1 and Figure 3.1 we describe the transfer matrix:

$$K_{pq}(\omega) = f(\omega)\sum_{j=1}^{M}\tau_j(\omega)G(\mathbf{x}_j,\mathbf{y}_p,\omega)G(\mathbf{x}_j,\mathbf{y}_q,\omega) \text{ for } p,q = 1,...,N. \tag{4.112}$$

It describes the response of transducer q due to a probing pulse being sent out by transducer p in the case of no multiple scattering, the scatterers are either weak or well separated[7]. At all times we work in the Fourier domain and define :

- $f(\omega)$ is the Fourier transform of the probing pulse.
- G is the background Green's function. It depends on the random medium and so takes into account the multipathing .
- $\tau_j(\omega)$ is the scattering coefficient of the j^{th} target.

By setting

$$\mathbf{g}(\mathbf{x}_m,\omega) = [G(\mathbf{x}_m,\mathbf{y}_1,\omega), G(\mathbf{x}_m,\mathbf{y}_2,\omega),...,G(\mathbf{x}_m,\mathbf{y}_N,\omega)]^T \tag{4.113}$$

we can rewrite this in terms of a matrix equation:

$$K(\omega) = f(\omega)\sum_{j=1}^{M}\tau_j(\omega)\mathbf{g}(\mathbf{x}_j,\omega)\mathbf{g}(\mathbf{x}_j,,\omega)^T \tag{4.114}$$

and take the singular value decomposition of $K(\omega)$:

- The N orthonormal eigenvectors of $K^\dagger K$ to be $v_p(\omega)$
- The N orthonormal eigenvectors of $KK^\dagger$ to be $u_p(\omega)$
- The square root of the eigenvalues of $K^\dagger K$ and $KK^\dagger$ are $\sigma_p(\omega)$. Where we reorder such that

$$\sigma_1(\omega) \geq \sigma_2(\omega) \geq ... \geq \sigma_M(\omega) > \sigma_{M+1}(\omega) \approx ... \approx \sigma_N(\omega) \approx 0 \tag{4.115}$$

Hence, $K = uDv^\dagger$ where D is a diagonal matrix with values $\sigma_1(\omega), \sigma_2(\omega), ..., \sigma_N(\omega)$.

The number of scatterers can be determined by the number of significant singular values.

If there are detectable targets in the medium, then the next step would be to locate them. We consider first that, due to the orthogonality of the vectors $\{u_p(\omega)\}$ that $\{u_1(\omega),...,u_M(\omega)\}$ form an orthonormal basis of the M dimensional subspace of C^N also spanned by $\{\mathbf{g}(\mathbf{x}_1,\omega),\mathbf{g}(\mathbf{x}_2,\omega),...\mathbf{g}(\mathbf{x}_M,\omega)\}$ with is orthogonal to all $u_i(\omega)$ for $M+1 \leq i \leq N$. We also note that if the target locations sufficiently far apart from each other that because $\mathbf{g}(\mathbf{x}_j,\omega)$ is a vector that illuminates the target locations that due to destructive interference and spacial decay of greens functions that $\mathbf{g}(\mathbf{x}_j,\omega)\mathbf{g}(\mathbf{x}_k,,\omega)^\dagger \approx 0$ for $j \neq k$.

[7] It is possible to describe the transfer matrix K in the multiple scattering case. Interested readers should see the appendix of Paper [6]

Thus because we have two orthogonal bases of the M dimensional subspace of C^N we can conclude that the the u_i are proportional to the illuminating vectors from the targets and we have:

$$u_i(\omega) \approx e^{i\phi(\omega)} \frac{\mathbf{g}(\mathbf{x}_j, \omega)}{|\mathbf{g}(\mathbf{x}_j, \omega)|} \tag{4.116}$$

for some $1 \leq j \leq M$ and arbitrary phase $\phi(\omega)$. This then gives that:

$$\sigma_r(\omega) \approx |f(\omega)||\tau(\omega)||\mathbf{g}(\mathbf{x}_j, \omega)|^2 \tag{4.117}$$

In a homogeneous medium, to find he location of the scatterers we could take a test point $\mathbf{x}_s$ and calculate:

$$u_r^\dagger(\omega) \frac{\mathbf{g}(\mathbf{x}_s, \omega)}{|\mathbf{g}(\mathbf{x}_s, \omega)|}. \tag{4.118}$$

Where, because of Equation 4.116 the inner product will be small unless $\mathbf{x}_s$ is close to one of the targets.

This however, will not work for random medium as the inner product wildly fluctuates for different values of $\mathbf{x}_s$. We hope that maybe the quantity is self averaging at that by integrating over frequency, as in lemma 4.2.1 we could solve this problem. However, this does not work in our case, because, recalling Equation 4.116, there is the existence of a phase factor. Previously this was cancelled by the time reversed wave but in this case it remains and it is not self averaging.

We rewrite our thoughts to give us a different view of the situation:

Lemma 4.3.1. *If $\boldsymbol{g}(\boldsymbol{x}_s, \omega)$ at search point $\boldsymbol{x}_s$ is orthogonal to the null space of $KK^\dagger$ then $\boldsymbol{x}_s$ coincides with one of the target locations $\boldsymbol{x}_j$ for some $1 \leq j \leq M$.*

Proof. The null space of $KK^\dagger(\omega)$ is spanned by the singular vectors $u_i(\omega)$ for $M+1 \leq i \leq N$ and is also orthogonal to the subspace spanned by $\{\mathbf{g}(\mathbf{x}_1, \omega), \mathbf{g}(\mathbf{x}_2, \omega), ...\mathbf{g}(\mathbf{x}_M, \omega)\}$.

Thus the vector $\mathbf{g}(\mathbf{x}_s, \omega)$ is orthogonal to the null space of $KK^\dagger(\omega)$ if and only if it lies in the subspace spanned by $\{\mathbf{g}(\mathbf{x}_1, \omega), \mathbf{g}(\mathbf{x}_2, \omega), ...\mathbf{g}(\mathbf{x}_M, \omega)\}$.

We recall that $\mathbf{g}(\mathbf{x}_j, \omega)\mathbf{g}(\mathbf{x}_k, , \omega)^\dagger \approx 0$ for $j \neq k$ and hence the set $\{\mathbf{g}(\mathbf{x}_s, \omega), \mathbf{g}(\mathbf{x}_1, \omega), ...\mathbf{g}(\mathbf{x}_M, \omega)\}$ is linearly independent.

Therefore if $\mathbf{g}(\mathbf{x}_s, \omega)$ is orthogonal to to the null space of $KK^\dagger(\omega)$ we have that $\mathbf{x}_s$ coincides with $\mathbf{x}_j$ for some $1 \leq j \leq M$. □

For an inhomogeneous medium, the vector $\mathbf{g}(\mathbf{x}_s, \omega)$ is randomly distributed and hence is not known. Instead, we approximate with the homogeneous case and G becomes the deterministic Green's function G_0:

$$\mathbf{g}_0(\mathbf{x}_s, \omega) = [G_0(\mathbf{x}_s, \mathbf{y}_1, \omega), G_0(\mathbf{x}_m, \mathbf{y}_2, \omega), ..., G_0(\mathbf{x}_s, \mathbf{y}_N, \omega)]^T. \tag{4.119}$$

Then taking inspiration from Lemma 4.3.1 we compute the projection of $\mathbf{g}_0(\mathbf{x}_s, \omega)$ onto the null space of $KK^\dagger(\omega)$, given by:

$$\mathcal{P}_N \mathbf{g}_0(\mathbf{x}_s, \omega) = \sum_{r=1}^{M} \left[u_r^\dagger(\omega) \mathbf{g}_0(\mathbf{x}_s, \omega) \right] u_r(\omega) - \mathbf{g}_0(\mathbf{x}_s, \omega) \tag{4.120}$$

for each frequency in the support of $f(\omega)$.

For the deterministic medium then $\mathbf{x}_p$ for $p = 1, ..., M$ are the zeros of $||\mathcal{P}_N \mathbf{g}_0(\mathbf{x}_s, \omega)||$ for any frequency. For a random medium, $\mathbf{g}_0(\mathbf{x}_s, \omega)$ can be quite different to $\mathbf{g}(\mathbf{x}_s, \omega)$ and it doesn't quite work. We recall that for statistical stability we needed to look at the wave, not in the frequency domain, but, in the space and time domain. This idea leads to the following algorithm which is given in Paper [6].

4.3.0.1 Time Domain Target Imaging Algorithm

To find $\mathbf{x}_j$ for some $1 \leq j \leq M$:

1. Start with some search point $\mathbf{x}_s$ and calculate $\mathbf{g}_0(\mathbf{x}_s, \omega)$
2. Compute its projection onto $\{u_i(\omega)$ for $M+1 \leq i \leq N\}$ by calculating $\mathcal{P}_N \mathbf{g}_0(\mathbf{x}_s, \omega)$ by Equation 4.120.
3. Normalise this by the singular value $\sigma_j(\omega)$ and return to the time domain:

$$\mathcal{F}^{(j)}(\mathbf{x}_s, t) = \int e^{-i\omega t} \sigma_j(\omega) \sum_{r=1}^{M} \left[u_r^\dagger(\omega) \mathbf{g}_0(\mathbf{x}_s, \omega) \right] u_r(\omega) d\omega - \int e^{-i\omega t} \sigma_j(\omega) \mathbf{g}_0(\mathbf{x}_s, \omega) d\omega \quad (4.121)$$

4. Define the deterministic arrival time to be:

$$t_p(\mathbf{x}_s) = \frac{|\mathbf{y}_p - \mathbf{x}_s|}{c_0} \quad (4.122)$$

5. Form the sum

$$\mathcal{G}^{(j)}(\mathbf{x}_s) = \sum_{p=1}^{N} (\mathcal{F}_p^{(j)}(\mathbf{x}_s, t_p(\mathbf{x}_s)))^2 \quad (4.123)$$

6. Define the functional

$$\mathcal{R}(\mathbf{x}_s) = \sum_{j=1}^{M} \frac{\min_{\mathbf{x}_s} \mathcal{G}^{(j)}(\mathbf{x}_s)}{\mathcal{G}^{(j)}(\mathbf{x}_s)} \quad (4.124)$$

Remark 15. In the homogeneous case we note that $\mathcal{G}^{(j)}(\mathbf{x}_s) \approx 0$ when $\mathbf{x}_s = \mathbf{x}_j$ for some $1 \leq j \leq M$. Thus in the inhomogeneous case we similarly take the estimates of the target locations of $\mathbf{x}_1, ..., \mathbf{x}_s$ to be the maxima of the objective functional $\mathcal{R}(\mathbf{x}_s)$

Remark 16. The normalisation by the singular value $\sigma_j(\omega)$ helps to give statistical stability of $\mathbf{F}^{(j)}(\mathbf{x}_s, t)$. To see this we consider the case of a single target ($M = 1$) and, using Equations 4.116 and 4.117, we can rewrite Equation 4.121 in the form:

$$\mathcal{F}(\mathbf{x}_s, t) = \mathcal{B}(\mathbf{x}_s, t) - \mathcal{A}(\mathbf{x}_s, t). \quad (4.125)$$

Where

$$\mathcal{A}(\mathbf{x}_s, t) = \int e^{-i\omega t} |f(\omega)||\tau_1(\omega)| \mathbf{g}_0(\mathbf{x}_s, \omega) \sum_{p=1}^{N} G(\mathbf{x}_1, \mathbf{y}_p, \omega) \overline{G(\mathbf{x}_1, \mathbf{y}_p, \omega)} d\omega \quad (4.126)$$

$$\mathcal{B}(\mathbf{x}_s, t) = \int e^{-i\omega t} |f(\omega)||\tau_1(\omega)| \mathbf{g}(\mathbf{x}_s, \omega) \sum_{p=1}^{N} G_0(\mathbf{x}_s, \mathbf{y}_p, \omega) \overline{G(\mathbf{x}_1, \mathbf{y}_p, \omega)} d\omega. \quad (4.127)$$

We notice that, like Γ as defined in Equation 4.6, the random Green's functions appear in complex conjugate pairs (approximately so in $\mathcal{B}$). Thus large random phases in the Green's functions cancel and like for Γ, we get statistical stability [8].

[8] We can create a clearer link to time reversal by considering, fist for $\mathcal{A}$ we take the expression:

$$|f(\omega)||\tau_1(\omega)| \sum_{p=1}^{N} G(\mathbf{x}_1, \mathbf{y}_p, \omega) \overline{G(\mathbf{x}_1, \mathbf{y}_p, \omega)}. \quad (4.128)$$

This can be interpreted as: an unknown target at $\mathbf{x}_1$ sends a pulse $|f(\omega)||\tau_1(\omega)|$ to the array. The array time-reverses and back-propagates and the field is measured again at $\mathbf{x}_1$. $\mathcal{A}(\mathbf{x}_s, t_p(\mathbf{x}_s))$ is then the field at test point $\mathbf{x}_s$ propagated to the array in a fictitious homogeneous medium.

For $\mathcal{B}$ we consider expression:

$$|f(\omega)||\tau_1(\omega)| \sum_{p=1}^{N} G_0(\mathbf{x}_s, \mathbf{y}_p, \omega) \overline{G(\mathbf{x}_1, \mathbf{y}_p, \omega)} \quad (4.129)$$

to have the interpretation: $\mathbf{x}_1$ sends a pulse $|f(\omega)||\tau_1(\omega)|$ to the array. Then we time reverse and back-propagate to $\mathbf{x}_s$ in a fictitious homogeneous medium. We don't yet have a self-averaging property. In fact, $\mathcal{B}(\mathbf{x}_s, t)$ is self-averaging because it is the propagation of the field given by Equation 4.129, evaluated at $\mathbf{x}_1$ back-propagated onto the array.

Remark 17. It is a statistically stable and relatively accurate Direction of Arrival (DOA) estimator for a narrow band array probing homogeneous media. The rough estimate of time given by Equation 4.122, means that that it is not necessarily a good approximation for the distance from the array. A more sophisticated arrival time estimate would help to obtain an improved range estimate.

4.3.0.2 Arrival Time Estimation

I will consider one possible method of improving the time estimation, which uses the Singular Value Decomposition. Suppose that the target at $\mathbf{x}_1$ is the strongest with singular value $\sigma_1(\omega)$ and corresponding singular vector $u_1(\omega)$ of $K(\omega)$ that we assume to be normalised but carries an arbitrary, frequency dependent phase. This singular vector is not statistically stable, but we can calculate N versions, coherent in time, by projecting the columns of the response matrix onto it:

$$u_1^{(p)}(\omega) = \left[u_1^\dagger(\omega)\mathbf{K}^{(p)}(\omega)\right] u_1(\omega). \tag{4.130}$$

Where $\mathbf{K}^{(p)}(\omega)$ is the p^{th} column of $K(\omega)$. We interpret $u_1^{(p)}$ as a singular vector of $K(\omega)$ with the phase of its p^{th} column. It is a known quantity which can be obtained by iterated time reversal, to focus on the strongest scatterer, and then back propagation to obtain $u_1^{(p)}$.

Subbing in the definition for K, see Equation 4.114, and the definition for u, see Equation 4.116. We find that for a single target in the domain[9]:

$$u_1^{(p)}(\omega) = f(\omega)\tau_1(\omega)G(\mathbf{x}_1, \mathbf{y}_p, \omega)\mathbf{g}(\mathbf{x}_1, \omega). \tag{4.131}$$

These we can synchronise and add them to get an effective singular vector:

$$\langle u_1(t)\rangle = \frac{1}{N}\sum_{p=1}^{N} u_1^{(p)}(t - \tau_p^{(1)}) \tag{4.132}$$

where we define $\tau_p^{(1)}$ to be the estimated travel times from transducer p to $\mathbf{y}_1$. Is defined so that the effective singular vector is close, in a least squares sense, to the values that it averages. Thus the $\tau_p^{(1)}$ are chosen to be the minimisers of:

$$\min_{\tau_p^{(1)}} \int_0^T \sum_{p=1}^{N} \left[u_1^{(p)}(t - \tau_p^{(1)}) - \frac{1}{N}\sum_{q=1}^{N} u_1^{(q)}(t - \tau_q^{(1)})\right]^2 dt = \min_{\tau_p^{(1)}} \int_0^T \sum_{p=1}^{N} \left[u_1^{(p)}(t - \tau_p^{(1)}) - \langle u_1(t)\rangle\right]^2 dt \tag{4.133}$$

where T is is large enough to capture most of the information.

To summarise the idea: we defined $\langle u_1(t)\rangle$, in an intuitively obvious way in terms of averaging and synchronisation, see Equation 4.132. We also conspired what it should satisfy, see Equation 4.133. By comparing the two we have found an estimation for travel times, what we were aiming for

We now worry about how to extend this to find arrival time estimates for a general scatterer in the domain, i.e. $\tau_p^{(j)}$, for $p = 1, ...N, \quad j = 1, ..., M$. We exploit the fact that if the targets are sufficiently far apart that the values $\sigma_j(\omega)$ for $j = 1, ..., M$ are well separated, i.e. have support over values of ω that form distinct sets. Thus one can choose an initial probing pulse $f(\omega)$ for each $j = 1, ..., M$ such that $\mathbf{x}_j$ is the strongest scatterer over the frequency band of the pulse. Thus arrival time estimates can be found between all scatterers and transducers.

4.3.0.3 Subspace arrival time analysis

We can now adapt the method described in Section 4.3.0.1 to take advantage of our improved estimated arrival times. For a search point $\mathbf{x}_s$ define a new objective functional :

$$\mathcal{R}_{SAT}(\mathbf{x}_s) = \sum_{j=1} \frac{\min_{\mathbf{x}_s} \mathcal{G}_{SAT}^{(j)}(\mathbf{x}_s)}{\mathcal{G}_{SAT}^{(j)}(\mathbf{x}_s)} \tag{4.134}$$

[9]If there is more than one target, the assumption that $\mathbf{x}_1$ is the strongest means that this, although not precise, is thought to be a good approximation

where

$$\mathcal{G}_{SAT}^{(j)}(\mathbf{x}_s) = \sum_{p=1}^{N} \left[\mathcal{F}_p^{(j)}(\mathbf{x}_s, t_p(\mathbf{x}_s))\right]^2 \left[\tau_p^{(j)} - t_p(\mathbf{x}_s)\right]^2 \tag{4.135}$$

and $\mathcal{F}$ defined as in 4.121. As before, we take the estimates of the target locations of $\mathbf{x}_1, ..., \mathbf{x}_s$ to be the maxima of the objective functional $\mathcal{R}(\mathbf{x}_s)$. In the Paper [6], it is shown that this imaging method is reliable and target locations estimated well even in the case of random media with strong inhomogeneities.

4.3.1 Alternative methods

The main limitation of this method is the assumption that each singular vector of K can be associated with a single scatterer. We label our vectors and singular values in equation 4.115 by ordering the singular values. But what if the order changes as frequency varies. This would need tracking, adding a large amount of extra complication to what is otherwise a relatively simple to describe method.

There are many other methods I could have considered for imaging in a random media. An example is the coherent interferometric (CINT) imaging method. As described in Paper [1], instead of directly back-propagating the received waves, the CINT method first computes cross-correlations of the recorded signals over chosen space-frequency windows and then back-propagates the local cross-correlations. As described in Paper [5] it estimates the source locations as the peaks of the image formed by superposing the array recordings delayed by travel times for the receivers to the imaging points. It is useful if there is some residual coherence in the array measurements that the method can exploit. The method is stable but often this is at the expense of resolution; there is over-smoothing taking place. Paper [5], discusses how l_1 optimisation can be used to improve resolution in inhomogeneous media when using the CINT method.

Chapter 5

Conclusion

I hope in this essay to have given a good overview of the principles of time-reversal and a variety of applications and extensions. I went on to describe in more detail the counter-intuitive phenomenon of 'super-resolution' in random media and why this is statistically stable. Finally, we briefly looked at a possible method for imaging in random media and gained a greater grasp of its complexities.

The essay bridges the experimental and the practical applications with mathematical theory and I hope to have given both justice. This field of interest is a good example of how mathematical analysis and rigour inspires and is inspired by experiments and real world applications.

There are many other avenues I could have discussed, some of which I pointed to throughout the essay. There is one big assumption I haven't yet addressed: I have focused solely on acoustic waves but of course there are many different times of waves and hence many more possible applications.

Electromagnetic waves are hugely significant category of waves we haven't considered and in fact the mathematics describing time reversal focusing is often simpler for EM waves because of the high frequencies. An example that I found interesting is given by Paper [16] which uses pulsed radar, electromagnetic waves in the microwave range, in time reversal experiments. It has the potential to improve detection in highly cluttered environments.

Another exciting potential application comes from quantum mechanics: all matter can be described by quantum wave-functions. A type of time reversal can occur when an electron wave function hits the boundary between a normal conductor and a superconductor, called Andreev reflection. This has hugely exciting possibilities and is an active area of research as can be seen in recent publications such as Paper [20] which talks about the production of a Quantum TRM and possible experimental directions. An area to watch in the future.

5.0.1 Acknowledgements

Many thanks to Dr Orsola Rath-Spivack for setting and assessing this essay and in doing so, introduced me to an interesting area of research.

Bibliography

[1] Habib Ammari, Elie Bretin, Josselin Garnier, and Vincent Jugnon. Coherent Interferometry Algorithms for Photoacoustic Imaging. *SIAM Journal on Numerical Analysis*, 50(5):2259–2280, 2012.

[2] B. E. Anderson, M. Griffa, C. Larmat, T. J. Ulrich, and P. A. Johnson. Time reversal. *Acoustics Today*, 4(1):5–16, 2008.

[3] Guillaume Bal and Leonid Ryzhik. Time Reversal and Refocusing in Random Media. *SIAM Journal on Applied Mathematics*, 63(5):1475–1498, 2003.

[4] Peter Blomgren, George Papanicolaou, and Hongkai Zhao. Super-resolution in time-reversal acoustics. *The Journal of the Acoustical Society of America*, 111(1):230–248, 2002.

[5] Liliana Borcea and Ilker Kocyigit. Imaging in Random Media with Convex Optimization. *SIAM Journal on Imaging Sciences*, 10(1):147–190, 2017.

[6] Liliana Borcea, George Papanicolaou, Chrysoula Tsogka, and James Berryman. Imaging and time reversal in random media. *Inverse Problems*, 18(5):1247–1279, 2002.

[7] Didier Cassereau and Mathias Fink. Time-Reversal of Ultrasonic Fields—Part III: Theory of the Closed Time-Reversal Cavity. *IEEE Transactions on Ultrasonics, Ferroelectrics, and Frequency Control*, 39(5):579–592, 1992.

[8] E. Cochard, C. Prada, J. F. Aubry, and M. Fink. Ultrasonic focusing through the ribs using the DORT method. *Medical Physics*, 36(8):3495–3503, 2009.

[9] Aj Devaney. Super-resolution processing of multi-static data using time reversal and MUSIC. *Journal of the Acoustical Society of America*, pages 1–25, 2000.

[10] Anthony J Devaney, Edwin A Marengo, and Fred K Gruber. Time-reversal-based imaging and inverse scattering of multiply scattering point targets. *The Journal of the Acoustical Society of America*, 118(5):3129–3138, oct 2005.

[11] M Fink. Time reversal of ultrasonic fields. I. Basic principles. *IEEE transactions on ultrasonics, ferroelectrics, and frequency control*, 39(5):555–566, 1992.

[12] M Fink. Time-reversed acoustics. *Scientific American (International Edition)*, 281(November 1999):91–113, 1999.

[13] Mathias Fink and Claire Prada. Acoustic time-reversal mirrors. *Inverse Problems*, 17(1), 2001.

[14] Jean Pierre Fouque, Josselin Garnier, André Nachbin, and Knut Sølna. Time-reversal refocusing for point source in randomly layered media. *Wave Motion*, 42(3):238–260, 2005.

[15] Yulia Hristova, Peter Kuchment, and Linh Nguyen. Reconstruction and time reversal in thermoacoustic tomography in acoustically homogeneous and inhomogeneous media. *Inverse Problems*, 24(5), 2008.

[16] José M.F. Moura and Yuanwei Jin. Detection by time reversal: Single antenna. *IEEE Transactions on Signal Processing*, 55(1):187–201, 2007.

[17] G Papanicolaou, L Ryzhik, and K Solna. Statistical stability in time reversal. *Siam Journal on Applied Mathematics*, 64(4):1133–1155, 2004.

[18] Claire Prada and Mathias Fink. Eigenmodes of the time reversal operator: A solution to selective focusing in multiple-target media. *Wave Motion*, 20(2):151–163, 1994.

[19] Orsola Rath-Spivack. Part III lectures: Direct and Inverse Scattering of Waves.

[20] Phillipp Reck, Cosimo Gorini, Arseni Goussev, Viktor Krueckl, Mathias Fink, and Klaus Richter. Towards a quantum time mirror for nonrelativistic wave packets. jan 2018.

[21] K Sølna and G Papanicolaou. Ray theory for a locally layered random medium. *Waves Random Media*, 10:151–198, 2000.

[22] B E Treeby and B T Cox. A k-space Green's function solution for acoustic initial value problems in homogeneous media with power law absorption. *J Acoust Soc Am*, 129(6):3652–3660, 2011.

[23] Zachary J. Waters and Paul E. Barbone. Discriminating resonant targets from clutter using Lanczos iterated single-channel time reversal. *The Journal of the Acoustical Society of America*, 131(6):EL468–EL474, 2012.

[24] Yuan Xu and Lihong V. Wang. Time Reversal and Its Application to Tomography with Diffracting Sources. *Physical Review Letters*, 92(3):033902, 2004.